A Szilikátipari Tudományos Egyesület lapja

építőanyag

Journal of Silicate Based and Composite Materials

A TARTALOMBÓL:

2020/4

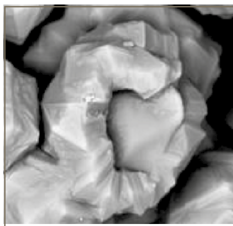

We are pleased to announce the organization of

ic-cmtp6

THE 6TH INTERNATIONAL CONFERENCE ON COMPETITIVE MATERIALS AND TECHNOLOGY PROCESSES

to be held in Hotel Palota in Miskolc-Lillafüred in May 3-7, 2021

The **ic-cmtp6** conference will be held in the wonderful palace of **Hotel Palota** in the exceptionally beautiful environment of **Beech Mountain** in **Miskolc-Lillafüred** in **Hungary**. In 2018 in the previous conference scientists had participated from **46** countries of **5** continents and the largest delegations have arrived from **Japan, Russian Federation, China, Czech Republic,** and **Korea**.

THE CONFERENCE SESSIONS

1. Advanced Ceramics and Nanoceramics
2. Advanced Composites and Nanocomposites
3. Advanced Materials for Bio- and Medical Applications
4. Advanced Materials for Extreme Applications
5. Advanced Nanomaterials and Nanocomposites
6. Advanced Optical Materials – Properties and Applications
7. Advanced Polymer-Clay Nanocomposites
8. Advanced Powder Metallurgy Materials
9. Advanced Processing and Characterization Methods for Nanocomposites
10. Bioelectronic Materials and Biosensors
11. Biomaterials Derived Ceramics and Nanocomposites
12. Clay Minerals and Organo-Clay Complexes
13. CO2 Capture and Fixing Materials and Methods
14. Glasses and Related Competitive Materials
15. Graphene – Properties and Applications
16. Hetero-Modulus and Hybrid Materials
17. Intelligence and Smart Materials – Structures, Properties and Applications
18. Interface as a Functional Material – Behavior, Function and Application
19. Light Weight Materials with Predesigned and Controlled Nanostructur
20. Materials and Methods to Capture and Fixing Radioactive Pollutants from Waters and Soils
21. Materials for Membranes and Catalysts
22. Materials for Biological Systems and Health
23. Materials for Energy Saving and Conservation
24. Materials for Harvesting Renewable Energy
25. Materials for Sensors and Actuators
26. Materials with Extreme Dynamic Strength
27. Mechanical Properties and Processing Technology of Advanced Materials
28. Minerals for Environmental and Medical Application
29. Nanomaterials Applied to Biomedical Applications and Nanomedicine
30. Nanomaterials for Electronic and Electrotechnical Applications
31. Novel Synthesis and Processing Technology
32. Polymer Derived Ceramics and Advanced Nanocomposites
33. Processing and Properties of Silicate Ceramics
34. Sol-Gel Technology in Materials Processing
35. Testing and Characterization of Materials – Methods, Equipment and Uncertainties
36. Traditional Ceramics and Building Materials
37. Traditional Ferrous and Nonferrous Metals

In case of pandemic quarantine of COVID-19 or other force majeure situation the conference ic-cmtp6 will be held in the same place in October 4-8, 2021.

Registration and further information: www.ic-cmtp6.eu

építőanyag

2020/4

Journal of Silicate Based and Composite Materials

TARTALOM

CONTENT

A finomkerámia-, üveg-, cement-, mész-, beton-, tégla- és cserép-, kő- és kavics-, tűzállóanyag-, szigetelőanyag-iparágak szakmai lapja
Scientific journal of ceramics, glass, cement, concrete, clay products, stone and gravel, insulating and fireproof materials and composites

A folyóiratot referálja · The journal is referred by:
EBSCO, ProQuest, Emerging Sources Citation Index, Google Scholar, INDEX COPERNICUS INTERNATIONAL, THOMSON REUTERS

A folyóiratban lektorált cikkek jelennek meg.
All published papers are peer-reviewed.
Kiadó · Publisher: Szilikátipari Tudományos Egyesület (SZTE)
Elnök · President: ASZTALOS István
1034 Budapest, Bécsi út 122–124.
Tel.: +36-1/201-9360 ▪ E-mail: epitoanyag@szte.org.hu
Tördelő szerkesztő · Layout editor: NÉMETH Hajnalka
Címlapfotó · Cover photo: GYURKÓ Zoltán

WWW.EPITOANYAG.ORG.HU
EN.EPITOANYAG.ORG.HU

Online ISSN: 2064-4477
Print ISSN: 0013-970x
INDEX: 2 52 50 ▪ 72 (2020) 117–150

Results of processing and complex interpretation of geophysical and satellite remote sensing data in the context of environmental management tasks

Aleksey S. AGEEV ▪ Saint-Petersburg Mining University, Geological Department, Russia ▪ ageevscience@gmail.com
László A. GÖMZE ▪ Institute of Ceramics and Polymer Engineering, University of Miskolc, Hungary ▪ femgomze@uni-miskolc.hu
Oleg L. KOTOV ▪ Quantorium, Center for Additional Education, Russia ▪ olegkotovrus@yandex.ru

Érkezett: 2020. 06. 30. ▪ Received: 30. 06. 2020. ▪ https://doi.org/10.14382/epitoanyag-jsbcm.2020.19

Aleksey S. AGEEV
is Ph. D. assistant professor at the department of Historical and Dynamics Geology of the Saint-Petersburg Mining University. Area of scientific interests is geological-geophysical methods of prospecting mineral deposits. He is author or co-author of 13 scientific papers.

László A. GÖMZE
is establisher and professor of the Department of Ceramics and Silicate Engineering in the University of Miskolc, Hungary. He is author or co-author of 2 patents, 6 books and more than 300 scientific papers.

Oleg L. KOTOV
is a student of "Quantorium", he works in the format of additional education in the field of engineering and IT technologies

Abstract

The article shows one of possible applications of the results of lineament analysis in the solution of environmental management tasks. The proposed methodology can be successfully applied to assess the mineralogical potential of the study areas regardless of the type of mineral deposit. Results can be used while planning investments by the industry of advanced materials and mining companies at the next stages of exploration. The authors have conducted a pre-processing and complex interpretation of remote sensing data in order to study the shape of individual faults and the spatial orientation of the whole network of dislocations. The final structural scheme was built in the results. The authors chose a fixed rectangular polygon within the Mongolo-Okhotsk fold belt (MOFB) as a reference area. By implementing algorithms of automated and visual methods of lineament analysis, it has been established that two groups of long-distance faults develop in the sub-latitudinal direction. Significant feature is the determination of a group of low-ranking lineaments that extend discordantly to the structure of MOFB. Identification of the form and spatial location of mapped lineament groups made it possible to identify potential areas for further detailed studies of the faults network and the spatial relationship of dislocations with mineral deposits.

Keywords: remote sensing, geophysics, geological mapping, tectonics, Mongol-Okhotsk fold belt data processing, environmental management tasks, faults, mineral deposits
Kulcsszavak: távérzékelés, geofizika, geológiai feltérképezés, tektonika, Mongol-Okhotsk vonal adatfelvétel, környezetgazdálkodási feladatok, hibák, ásványi lerakódások

1. Introduction

One of a number of the most important factors ensuring sustainable development in the modern world is rational natural resource management. Today's industrial progress of advanced materials is provided by environmental management. Many works are devoted to the use of natural raw materials for advanced materials [1-4]. We can't say this about the methods of possible applications of the results of lineament analysis in solving environmental management problems.

The main goal of government programs in this field is increasing the country's mineral resource base through the development of new areas of interest or the reappraisal of existing deposits. To achieve this, new technologies and methods for prospecting, exploration and production of minerals are being introduced into the mining industry. The use of integrated solutions for the tasks of geological mapping and minerageny studies provides for qualitative improvement of the results.

To date, the fastest evolving method of obtaining new geological information is the processing of remote sensing data. This analysis performs during processing space images, data from geophysical surveys and geological mapping. The main interpretation unit in the analysis process is lineament [5, 6]. The result of this work is the diagram of lineaments spatial relation. They indirectly characterize fault and blocking tectonics of the surveyed region [7, 8]. Mineral deposits connect to areas with high concentration of faulting. In this regard, the analysis of positional relation of the main fault systems in the surveyed area is of crucial importance.

There are two different approaches to conducting lineament analysis: automated (via specialized software) and visual. Both of these methods have proven effective in solving various prospecting problems [9-12]. Automated lineament analysis is excellent in regions with a simple geological structure (regular or monoclinal bedding) [13, 14]. The situation becomes more complicated if several stages of tectogenesis are evident. The results of visual lineament analysis can be considered closer to the actual geological situation, since the process implies the knowledge of geological structure and the spread of faulting patterns in the survey area. Apart from qualitative results, this kind of lineament analysis takes a lot of time and significantly slows down the processing when a large amount of geological and geophysical data is engaged.

In this regard, the most urgent task is to develop an effective method for processing remote sensing data, which would combine the results of both kinds of analysis. As the work outcome, a diagram of faulting patterns positional relation in the survey region should be developed.

To solve the tasks, authors conducted two kinds of analysis of the remote sensing data complex within the field survey site located in the tectonically active Mongol-Okhotsk fold belt (MOFB) in Russia. Within this geological structure, a large number of mineral deposits are concentrated [15].

2. A Brief History of Geological Evolution

The main structural elements of the earth's crust in surveyed region are the Aldanian Shield and the Mongol-Okhotsk folded belt (MOFB) (*Fig. 1*).

The history of the region geological evolution is long and extremely complex. Most scientists consider MOFB is an accretional structure as the result of collision on the southern periphery of Siberian platform. The formation of MOFB modern structure is associated with the closure of the Paleo-Asian Ocean at the end of the Cimmerian (Jurassic-Cretaceous) orogeny cycle. Results of geological investigations show that Late – Middle – Proterozoic complexes and Precambrian basement were mapped within the polygon. The dominant orientation of folded structures is sub-latitudinal.

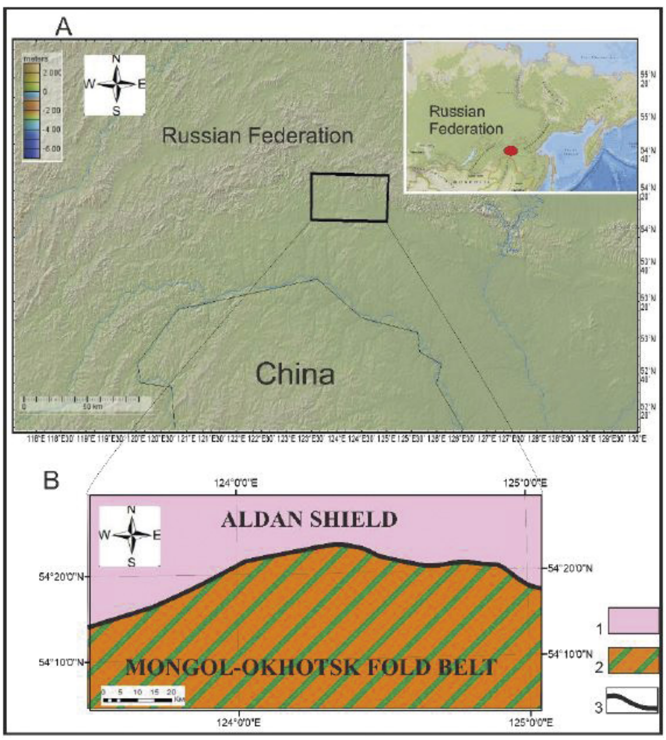

1. ábra A vizsgált terület földrajzi elhelyezkedése és szerkezeti térképe (egyszerűsítve [16])
Jelmagyarázat: 1 - konszolidált kéreg a Mezo-Proterosoicus kezdete előtt; 2 - Tektonikus újrafeldolgozás a Korai Krétakorban; 3 - Fő hiba

Fig. 1 Geographical location and structural map of researched area (simplified from [16])
Legend: 1 – Consolidated crust by the beginning of the Meso-Proterosoic; 2 – Tectonic reworking in Early Cretaceous; 3 – Main fault

3. Methods

The total amount of work was divided into several major phases. The first phase includes the preparation of source material and the formation of a database. The geological data bank was formed via the Esri's ArcMap 10.3 software. The base materials were linked together and placed in a single coordinate system prior to input, which facilitated subsequent minimization of spatial errors when conducting lineament analysis. The work featured the following: Geological map of the Russian Federation and adjacent areas [16], Tectonic map of Northern-Central-Eastern Asia [17], Initial geophysical remote sensing data (scale 1: 500 000) courtesy of the "A. P. KARPINSKY RUSSIAN GEOLOGICAL RESEARCH INSTITUTE" (FGBU «VSEGEI»)" [18], Multispectral image Landsat -8 (image courtesy of the U.S. Geological Survey).

Intermediate processing of geophysical fields was carried out via Golden Software's Surfer 12 application. Horizon and full gradients were calculated; local and regional field components were distinguished. The obtained data was added sequentially to the geological data bank for further analysis.

Preliminary processing of space images was carried out via Harris Geospatial Solutions' ENVI 5.1 software. At the first phase of preparation, the Landsat 8 multispectral space image was subjected to radiometric calibration to prevent radiometric signal bias. The atmospheric correction was carried out to minimize the effect of distortion of air layer between the earth's surface and radar. The final phase in preparing a space image is the procedure for increasing the resolution of standard channels (30 m) according to the panchromatic channel (15 m) — pansharpening.

At the next phase, an automatic and visual lineament analysis of all informative layers was carried out and monomethod lineament diagrams were compiled.

The final phase was the conduct of a comprehensive interpretation of data, which includes defining the nature of lineaments mapped by remote sensing. At this phase, the verification of monomethod diagrams by comparing with each other and with other sources of information (geological and tectonic maps, diagrams, seismic origins, etc.) was of crucial significance. These procedures were performed interactively. It is imperative that the verification of monomethod diagrams include the validation of source of initial data and the lineaments obtained from it. The results of automatic analysis of geophysical data should be compared with similar resulting diagrams of visual analysis. The same is applicable to data collected from space images.

Comparison of lineament diagrams with each other was the first element in the chain of comprehensive interpretation of data aiming to remove the lineaments distinguished by one source only. The remaining lineaments were locked (grouped or merged) and transferred to a separate information layer. The diagram formed as a result of these operations was subjected to further verification using base materials and comparing with summarized and generalized tectonic maps and diagrams. The outcome was the summary diagram of lineaments positional relation in the survey area.

3.1 Automated Lineament Analysis

One of the most common methods for conducting lineament analysis is the algorithm of image "edge finding". This algorithm is implemented in the PCI GeoAnalyst, Geomatica (LINE module) software. For this study, the LINE module of PCI Geomatica software was used. The procedure for lineaments automatic extracting consists of two phases. The first is automatic "edge finding", i.e. search for information about areas of sharp transients in values of neighboring pixels. At the first step of processing, the radius (in pixels) of low-frequency Gaussian filter (RADI) is set to "soften" and blur the image. Next, the gradient value is set, which should be considered as a threshold value when moving to a neighboring pixel. Filtered data is analyzed for a set gradient to obtain a binary image. After analyzing the binary image, curves are extracted from it, and subsequently converted into vector graphic format by "fitting" straightened segments to them. The maximum error between the shape of these segments and original curve is set by processor. The listed parameters were set in an experimental manner for geophysical fields and space image separately (*Tables 1* and *2*). The result of this work was monomethod diagrams of lineaments positional relation.

Parameter	Value
RADI	10
GTHR	25
LTHR	30
FTHR	3
ATHR	45
DTHR	10

1. táblázat A LINE paraméterei a geofizikai adatokhoz
Table 1 LINE's parameters for geophysical data

Parameter	Value
RADI	3
GTHR	130
LTHR	30
FTHR	3
ATHR	45
DTHR	10

2. táblázat A LINE paraméterei a Landsat-hoz
Table 2 LINE's parameters for Landsat

3.2 The Results of Automated Lineament Analysis

High informative results were received by geophysical data processing. (*Fig. 2*). Lineaments have a predominantly sub-latitudinal and SW-NE spatial orientation. Analysis of other materials of geophysical fields and its transformants indicates that the mapped lineaments have a similar spatial orientation. Their largest number is evident in the southern part of the site. There they form chains stretching in the sub-latitudinal direction. These conclusions are confirmed by rose diagrams and lineament density calculations.

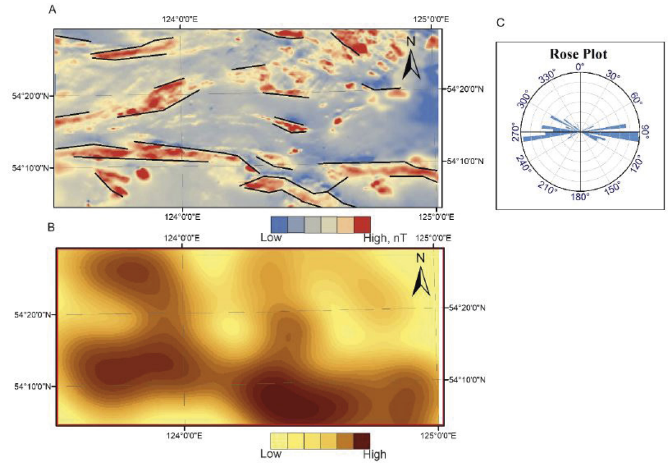

2. ábra Az automatizált lineáris elemzés (LINE) eredményei. Csak az 1000 métert meghaladó vonalak. A - mágneses mező anomália; B - a vonalak térbeli sűrűsége; C - Rose plot

Fig. 2 Results of the automated lineament analysis (LINE). There are only lineaments longer 1000 meters. A – anomaly magnetic field; B – Spatial density of lineaments; C – Rose plot

The least informative were the results of the gravity field automated analysis. This can be explained by the absence of intense anomalies and the smooth variation of field over a large area.

The lineament diagram of a space image differs significantly from the rest. Here it is difficult to trace one predominant direction of the lineament strike, but several can be distinguished: WSW, NNE, ENE. An analysis of density plot indicates that the concentration of lineaments is evident in the southern and northwestern parts of the site, which partially correlates with the results of processing data from geophysical fields (*Fig. 3*).

While analyzing the overall picture of the lineament's positional relation, it can be noted that there are both similar and distinctive features. The predominant sub-latitudinal strike of lineaments and their increased concentration in the southern part of the site were identified.

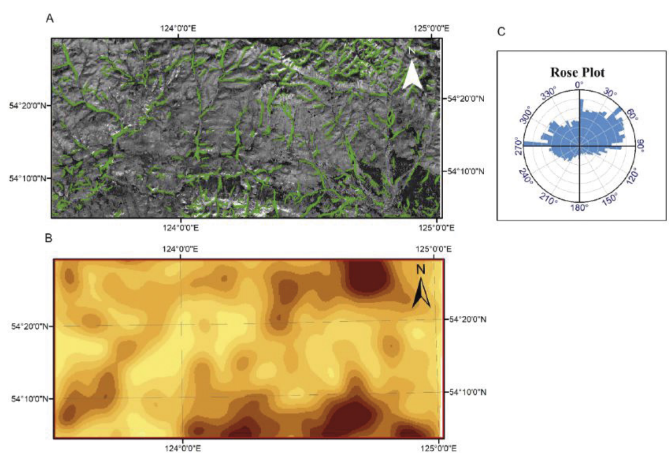

3. ábra Az automatizált lineáris elemzés (LINE) eredményei. Csak az 1000 métert meghaladó vonalak. A - LANDSAT 8 (5. sáv); B - a vonalak térbeli sűrűsége; C - Rose plot

Fig. 3 Results of the automated lineament analysis (LINE). There are only lineaments longer 1000 meters. A – LANDSAT 8 (Band 5); B – Spatial density of lineaments; C – Rose plot

3.3 Visual Lineament Analysis

The main requirement for the process of conducting visual lineament analysis was to maintain a strict spatial reference. In this regard, the ArcMap 10.5 and Corel Draw X9 (with the coordinate grid set) software was used. Lineaments were distinguished via direct decryption method for all data types. The following was considered the signs of lineaments on geophysical fields and transformants:

- Changes in color and tone characteristics of the field
- Areas of high field gradients
- A sharp transient in direction of neighboring isometric curves, as well as their interruption

It should be noted that this approach enables ranking the distinguished lineaments while processing. The first two signs correspond to long and large lineaments, which can be interpreted as regional faults. In addition to a large extent, they are characterized by high contrast of display in the fields. The third sign makes it possible to map segments of significantly lesser extent and contrast of display. Such lineaments are considered local faulting (*Fig. 4*).

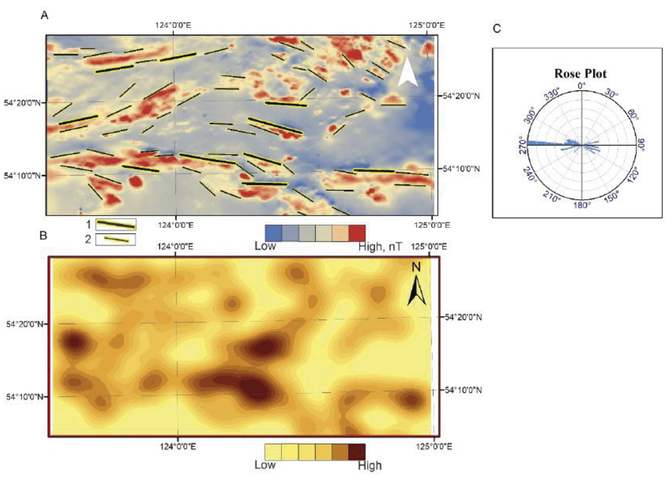

4. ábra A vizuális vonal-elemzés eredményei. A - mágneses mező anomália: 1 - 1. rangú vonalak, 2 - 2. rangú vonalak; B - a vonalak térbeli sűrűsége; C - Rose plot
Fig. 4 Results of the visual lineament analysis. A – Anomaly magnetic field: 1 – 1st rank lineaments, 2 – 2nd rank lineaments; B – Spatial density of lineaments; C – Rose plot

3.4 Results of Visual Analysis

A similar picture of lineaments' positional relation is observed in all monomethod lineament diagrams whose sources were geophysical fields and transformants. General sub-latitudinal strike is evident. A group of lineaments of SW-NE strike stands out in the northwestern part of surveying panel. The number of lineaments per area unit is approximately the same throughout the site with a slight increase in the southern part.

The signs of lineaments in the space image were natural straightened land forms, including riverbeds, mountain ranges, long narrow basins. The initial multispectral image in a combination of 7, 4, and 2 channels was selected for analysis (*Fig. 5*). This combination of channels, as was shown by researchers, is the most informative when mapping lineaments that could be interpreted as faulting [19, 20]. Further, lineaments were divided into two ranks.

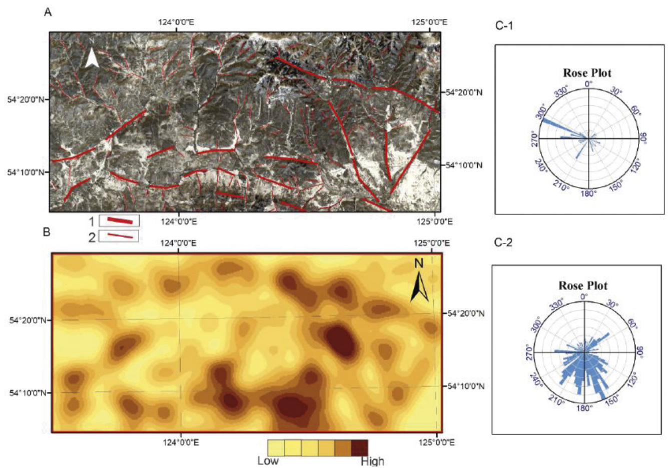

5. ábra A vizuális vonal-elemzés eredményei. A - LANDSAT 8 (7,4,2 sávok): 1 - 1. rangsor vonalak, 2 - 2. rangsor vonalak; B - a vonalak térbeli sűrűsége; C-1 - Rose plot az 1. rang; C-2 - Rose plot a 2. rang
Fig. 5 Results of the visual lineament analysis. A – LANDSAT 8 (7,4,2 bands): 1 – 1st rank lineaments, 2 – 2nd rank lineaments; B – Spatial density of lineaments; C-1 – Rose plot for 1st rank lineaments; C-2 – Rose plot for 2nd rank lineaments

The positional relation pattern of lineaments according to space image differs from the results of the same analysis of geophysical fields and transformants. Lineaments of the 1st and 2nd ranks are characterized by different orientations. The primary strike of the 1st rank lineaments is the NW direction. This can be explained by the general orientation of river system in this area. It is difficult to identify the general strike for the 2nd rank lineaments, since they are approximately equally distributed between the SE and SW directions. This fact is of great interest and the need for further research, since there are no significant differences in the spatial orientation of lineaments according to remote geophysical survey. An increased number of straightened land sections per area unit is observed in the SE and NE parts of the site.

3.5 Comprehensive Interpretation and Summary Diagram

At the final phase, a comprehensive interpretation of the obtained data was carried out and a diagram was developed reflecting the positional relation of primary and secondary lineaments in the survey area (*Fig. 6*).

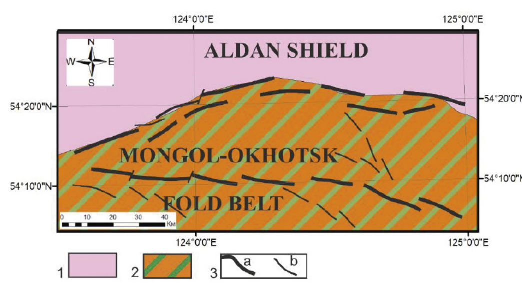

6. ábra A kapott vonalrendszer. Jelmagyarázat: 1 - konszolidált kéreg a Mezo-Proterosoicus kezdete előtt; 2 - Tektonikus újrafeldolgozás a Korai Krétakorban; 3 - 3a - 1. rangú vonás, 3b - 2. rangú vonás
Fig. 6 Resulting scheme of lineaments. Legend: 1 – Consolidated crust by the beginning of the Meso-Proterosoic; 2 – Tectonic reworking in Early Cretaceous; 3 – Lineaments: 3a – 1st rank lineament, 3b - 2nd rank lineaments

Based on the results of summary diagram analysis, several groups of lineaments were distinguished that strike generally in the sub-latitudinal direction. The northern group was mapped along the area of development of the deep fault, which is the structural boundary between MOFB and the Aldanian Shield. It should be noted that according to the results of interpretation there was not distinguished any single fault structure, but the extended fragments (up to 5,000 m) oriented in the adjacent axe were mapped. The southern group of lineaments is represented by extended (up to 4000 m) faults. An interesting feature is the presence of a group of 2nd rank lineaments, the strike of which (NW-SE) radically differs from other groups of faulting. The authors suggest that the faults of this group can be parts of the general deep faults and may spatially connect the southern and northern branches of rifting, thereby combining them into a single faulting pattern.

4. Conclusions

Thus, the summary diagram of positional relation of faulting in the survey area results the comprehensive method of remote sensing data processing and interpretation. Two general faulting groups with a sublatitudinal orientation were distinguished. No single for general fault structure was registered, but several faults of the same rank were distinguished within these groups. An important feature of the summary diagram is the presence of a group of 2nd rank faults with NW-SE strike, located between the general rifting groups.

The results obtained indicate that the most promising areas for prospecting and exploration for mineral deposits are the southern and northern fault propagation groups distinguished in the course of work. In addition, the area of propagation of 2nd rank faulting patterns is also of heightened interest.

Acknowledgements

The publication has been prepared in the context of a government order of Russia on «Development of inter-disciplinary trends in the complex development of the Earth's interior and nature preservation» # 075-03-2020-127\1.

References

[1] Kotova, O. B. – Shushkov, D. A. – Gömze, A. L. – Kurovics, E. – Ignatiev, G. V. – Sitnikov, P. A. – Ryabkov, Y. I. – Vaseneva, I. N. (2019): Composite materials based on zeolite-montmorillonite rocks and aluminosilicate wastes. Építőanyag–JSBCM, Vol. 71, No.4, pp. 125–130. https://doi.org/10.14382/epitoanyag-jsbcm.2019.22

[2] Shchemelinina T.N., Gömze A.L., Kotova O.B., Ibrahim J.E.F.M., Shushkov D.A., Harja M., Ignatiev G.V. Anchugova E.M. (2019): Clay- and zeolite-based biogeosorbents: modelling and properties Építőanyag–JSBCM, Vol. 71, No.4, pp.131–137. p. https://doi.org/10.14382/epitoanyag-jsbcm.2019.23

[3] Kurovics, E. – Kotova, O. B.– Gömze, A. L.– Shushkov, D. A. – Ignatiev, G. V. – Sitnikov, P. A. – Ryabkov, Y. I. – Vaseneva, I. N. – Gömze, L. N. (2019): Preparation of particle-reinforced mullite composite ceramic materials using kaolin and IG-017 bio-origin additives Építőanyag–JSBCM, Vol. 71, No.4, pp.114–119. https://doi.org/10.14382/epitoanyag-jsbcm.2019.20

[4] Ibrahim, J. E. F. M. – Gömze, A. L. – Kotova, O. B. – Shchemelinina, T. N. – Shushkov, D. A. – Ignatiev, G. V. – Anchugova, E. M. (2019): The influence of composition, microstructure and firing temperature on the density, porosity, and shrinkage of new zeolite-alumina composite material. Építőanyag–JSBCM, Vol. 71, No.4, pp.120–124. https://doi.org/10.14382/epitoanyag-jsbcm.2019.21

[5] Hobbs, W. H. (1904): Lineaments of the Atlantic border region. Geol Soc Am Bull, Vol. 15, pp. 483–506, https://doi.org/10.1130/GSAB-15-483

[6] O'Leary, D. W. – Friedman, J. D. – Pohn, H. A. (1976): Lineament, linear, lineation: some proposed new standards for old terms, Bull Geol Soc Am, Vol. 87, pp.1463–1469, https://doi.org/10.1130/0016-7606(1976)87<1463:LLLSPN>2.0.CO;2

[7] Ageev, A.S. (2018): Osobennosti glubinnogo stroeniya Baikal-Stanovoi regional'noi sdvigovoi zony po resul'tatam complexnoi interpretacii geologo-geophysicheskih dannyh. Candidate Dissertation (Features of the deep structure of the Baikal-Stanovoi regional shift zone as a result of complex interpretation of geological and geophysical data. Cand. Diss.), Moscow, 96 p. (in Russian).

[8] Egorov, A. S. (2004): Glubinnoe stroenie i geodinamika litosfery Severnoj Evrazii: Po rezul'tatam geologo-geofizicheskogo modelirovaniya vdol' geotraversov Rossii. Doctor Dissertation (Depth structure and geodynamics of the lithosphere of Northern Eurasia: Based on the results of geological and geophysical modeling along Russian geotravers, Doct. Diss.), Saint-Petersburg, 390 p. (in Russian).

[9] Sarup, J. – Muthukumaran, M. – Nitin, M. – Peshwa, V. (2006): Study of tectonics in relation to the seismic activity of the Dalvat area, Nasik District, Maharashtra, India using remote sensing and GIS techniques. Int J Remote Sens, Vol. 27, Issue 12, pp.2371–2387.

[10] Zhantayev, Zh. – Bibossinov, A. – Fremd, A. – Talgarbayeva, D.– Kikkarina, A. (2017): Automated lineament analysis to assess the geodynamic activity areas, Procedia Computer Science, Vol. 121, pp. 699-706, https://doi.org/10.1016/j.procs.2017.11.091

[11] Yamusa, I. B. – Yamusa, Y. B. – Danbatta, U. A. (2018): Geological and structural analysis using remote sensing for lineament and lithological mapping, IOP Conference Series: Earth and Environmental Science, Vol. 169, 9th IGRSM International Conference and Exhibition on Geospatial & Remote Sensing (IGRSM 2018) 24–25 April 2018, Kuala Lumpur, Malaysia, 1-9 pp. https://doi.org/10.1088/1755-1315/169/1/012082

[12] Mathew, J. – Jha, V. K. – Rawat, G. S. (2007): Application of binary logistic regression analysis and its validation for landslide susceptibility mapping in part of Garhwal Himalaya, India. Int J Remote Sens, Vol. 28, Issue 10, pp.2257–2275, https://doi.org/10.1080/01431160600928583

[13] Mostafa, M. E. – Bıshta, A. Z. (2005): Significance of lineament patterns in rock unit classification and designation: a plot study on the Gharib-Dara area, northern astern Desert, Egypt. Int J Remote Sens, Vol. 26, Issue 7, pp.1463–1475, https://doi.org/10.1080/01431160410001705088

[14] Masoud, A. – Koike, K. (2006): Tectonic architecture through Landsat-7 ETM/SRTM DEM-derived lineaments and relationship to the hydrogeologic setting in Siwa region, NW Egypt. J Afr Earth Sci, Vol. 45, Issues 4-5, pp. 467–477, https://doi.org/10.1016/j.jafrearsci.2006.04.005

[15] Kadashnikova, A. Y. – Sorokin, A. A. – Ponomarchuk, V. A. (2019): Distribution of Mineralization, Ages, and Sources of the Malomyr Gold Deposit, Eastern Part of the Mongol–Okhotsk Fold Belt, Geology Ore Deposits, Vol. 61, Issue, 1–13 pp. https://doi.org/10.1134/S1075701519010045

[16] Geologicheskaya karta Rossii i prilegayushchih akvatorij. Masshtab 1 : 2 500 000 (2015): (Geological map of the Russian Federation and adjacent areas at scale 1 : 2 500 000), Saint-Petersburg, "VSEGEI", p. 60. (In Russian).

[17] Tectonic map of Northern – Central – Eastern Asia and Adjacent Areas at scale 1: 2 500 000, Saint-Petersburg, "VSEGEI", 2014.

[18] Cifrovoj katalog Gosudarstvennyh geologicheskih kart RF mastaba 1:1000000 (tret'e pokolenie) (Digital catalog of the Geological maps of Russia (scale 1:1 000 000) 3rd edition). Available at https://www.vsegei.ru/ru/info/pub_ggk1000-3/ (In Russian).

[19] Ageev, A. S. – Ilalova, R. K. – Talovina, I. V. – Durjagina, A. M. (2019): A link between spatial distribution of the active tectonic dislocation and groundwater water resources in the Baikal-Stanovaya shear zone), Gornyj informacionno-analiticheskij bjulleten', No.5, pp.173-180. https://doi.org/10.25018/0236-1493-2019-05-0-173-180

[20] Davydenko, A. Ju. – Ajkasheva, N. A. – Buhalov, S. V. – Davydenko, Ju.A. (2017): Rezul'tat kompleksirovanija dannyh impul'snoj jelektrorazvedki i ajeromagnitorazvedki pri poiskah podzemnyh vod na juge Jakutii (Result of pulse electrical prospecting data integration and aeromagnetic research for underground's water survey in South Yakutia), Zapiski Gornogo instituta, Vol. 224, pp.156-162. https://doi.org/10.18454/PMI.2017.2.156

Ref.:
Ageev, Aleksey S. – **Gömze**, László A .– **Kotov**, Oleg L.: *Results of processing and complex interpretation of geophysical and satellite remote sensing data in the context of environmental management tasks*
Építőanyag – Journal of Silicate Based and Composite Materials, Vol. 72, No. 4 (2020), 118–122. p.
https://doi.org/10.14382/epitoanyag-jsbcm.2020.19

TURKEYTRIB 2020 3rd INTERNATIONAL CONFERENCE ON TRIBOLOGY

POSTPONED TO DECEMBER 2020

June 18-20 2020

CONFERENCE VENUE: Elite World Prestige Hotel
ADDRESS: Şehit Muhtar Caddesi No:40, 34435 Taksim Istanbul-TURKEY
WELCOME TO TURKEYTRIB 2020!

We are very pleased to announce that the 3rd International Conference on Tribology TURKEYTRIB 2020 will be held from 18 to 20 June 2020 at the Elite World Prestige Hotel Taksim-İstanbul-TURKEY. The scope of this conference embraces the state of art and future trends in tribology research and application, emphasizing the necessity of facilitation intellectual collaboration across both disciplinary and national-international boundaries. The main objective of the conference is to provide a unique opportunity of presenting and discussing recent developments in different aspects of Tribology and strengthen the linkage between academia and industry. The conference consists of scientific sessions, symposia on specific topics, exhibitions and various collateral events. Turkish and Foreign groups of experts will have chance to share information and get in touch with other groups in all part of Tribology. Nowadays these aspects are becoming more and more important both in respect of human life and environment.

– SPECIAL ISSUE (Web of Science Core Collection-Emerging Sources Citation Index): Selected high-quality papers (10) presented at the TurkeyTrib'20 conference will be selected and invited to submit their contributions for Special Issue publication in Építőanyag - Journal of Silicate Based and Composite Materials. (SCIE; Impact Factor 1.079 (2018). The submission due is 30 June 2020.

www.turkeytribconference.com/index.php/en/

TURKEYTRIB 2020
3rd INTERNATIONAL CONFERENCE TRIBOLOGY
18-20 JUNE
ELITE WORLD PRESTIGE HOTEL-TAKSIM
ISTANBUL-TURKEY

Preparation and electromagnetic microwave adsorption performances of porous nanocomposite self-assembled by $CoFe_2O_4$ nanoparticles and diatomite

Haodong HUANG ▪ Key Laboratory of Solid Waste Treatment and Resource Recycle of Ministry of Education, School of Environment and Resource, Southwest University of Science and Technology, China
Meng HE ▪ Key Laboratory of Solid Waste Treatment and Resource Recycle of Ministry of Education, School of Environment and Resource, Southwest University of Science and Technology, China
Olga B. KOTOVA ▪ Institute of Geology, Komi Science Center, Ural Branch of the Russian Academy of Sciences, Russian Federation
Yevgeny GOLUBEV ▪ Institute of Geology, Komi Science Center, Ural Branch of the Russian Academy of Sciences, Russian Federation
Faqin DONG ▪ Key Laboratory of Solid Waste Treatment and Resource Recycle of Ministry of Education, School of Environment and Resource, Southwest University of Science and Technology, China
László A. GÖMZE ▪ Institute of Ceramics and Polymer Engineering, University of Miskolc, Miskolc, Hungary, IGREX Engineering Service Ltd
Emese KUROVICS ▪ Institute of Ceramics and Polymer Engineering, University of Miskolc, Hungary
Rui LV ▪ Key Laboratory of Solid Waste Treatment and Resource Recycle of Ministry of Education, School of Environment and Resource, Southwest University of Science and Technology, China
Shiyong SUN ▪ Key Laboratory of Solid Waste Treatment and Resource Recycle of Ministry of Education, School of Environment and Resource, Southwest University of Science and Technology, China
▪ shysun@swust.edu.cn
Érkezett: 2020. 06. 30. ▪ Received: 30. 06. 2020. ▪ https://doi.org/10.14382/epitoanyag-jsbcm.2020.20

Abstract
The efficient nanocomposite of $CoFe_2O_4$ diatomite for electromagnetic microwave adsorption was assembled by $CoFe_2O_4$ nanoparticles (NPs) and diatomite via a simple citric acid-nitrate sol-gel auto-combustion method. The electronic microscopy results show that the magnetic $CoFe_2O_4$ NPs are uniformly dispersed in the surface and porous structure of diatomite to form stable $CoFe_2O_4$/diatomite nanocomposite. The magnetic and dielectric properties with various mass ratios of $CoFe_2O_4$ to diatomite was investigated. It was showed that nanocomposite of $CoFe_2O_4$/ diatomite has strong superparamagnetic and electromagnetic microwave absorbing properties with optimized conditions of coercive force of 837.07 Oe, the saturation magnetization of 96.5 emu/g, and the remanence ratio (Mr/Ms) of 0.52, respectively. The maximum reflection loss is -12dB, and <-10dB frequency ranges from 10Hz to 12Hz when the ratio of $CoFe_2O_4$ to Diatomite is 1:10. The results indicate that $CoFe_2O_4$/diatomite composites can be used as the highly efficient microwave absorption materials, which expanded the application field of diatomite-based functional nanomaterials.
Keywords: diatomite; $CoFe_2O_4$, electromagnetic microwave adsorbent, nanocomposite, porous minerals
Kulcsszavak: kovaföld, $CoFe_2O_4$, elektromágneses mikrohullámú adszorbens, nanokompozitot, porózus ásványok

1. Introduction

With the rapid development of electronic technologies, the electromagnetic interference (EMI) caused by electromagnetic microwaves (EMW) is becoming serious problems. The harmful electromagnetic radiation (EM radiation or EMR) not only affects sensitive electronic equipment, but also harmful to human health [1, 2]. In order to reduce the impact of EMW, scientists pay much attention to explore and design high-performance electromagnetic wave absorbing materials with properties of lightweight, wide frequency range and low cost [3-7]. The EM absorbing material has been applied not only

Haodong HUANG
is a final year student of innovation programe of Resource Recycling in Southwest University of Science and Technology of China under supervision of Prof. Shiyong Sun.

Meng HE
is a second year postgraduate student of Geological Resources and Geological Engineering in Southwest University of Science and Technology of China under supervision of Prof. Shiyong Sun.

Olga B. KOTOVA
is Head of Laboratory of Technology of Mineral Raw, Institute of Geology Komi SC UB Russian Academy of Sciences. Author and co-author of 10 books, 4 patents and more than 200 scientific articles. President of ICAM-2019. The member of Science Council of Russian Mineralogical Society

Yevgeny A. GOLUBEV
is leading researcher of Laboratory of Experimental Mineralogy, Institute of Geology Komi SC UB Russian Academy of Sciences. Author and co-author of 5 books and more than 60 scientific articles. The member of Russian Mineralogical Society.

Faqin DONG
is a professor of School of Environment and Resource of Southwest University of Science and Technology of China. He is author or co-author of more than 300 scientific papers.

László A. GÖMZE
is establisher and professor of the Department of Ceramics and Silicate Engineering in the University of Miskolc, Hungary. He is author or co-author of 2 patents, 6 books and more than 300 scientific papers.

Emese KUROVICS
is graduated from the University of Miskolc, Department of Ceramics and Silicate Engineering as a material engineer, where she continues her study as PhD student under supervision of Prof. L. A. Gömze.

Rui LV
is a second year PhD student of Environment Science and Technology in Southwest University of Science and Technology of China under supervision of Prof. Shiyong Sun.

Shiyong SUN
is a professor of School of Environment and Resource of Southwest University of Science and Technology of China. He is author or co-author of more than 80 scientific papers.

in the stealth technology of military, but also the ordinary commercial productions in all aspects to effectively reduce the reflection and transmission of EMW by converting EM into thermal energy [7-9]. Generally, the typical electromagnetic wave absorbents are constructed by embedding an EMW adsorbent into a host matrix, whose microwave adsorbing properties are primarily determined by the suspended materials.

Ferrite is one of the main frequently used microwave absorbing materials, which can efficient absorbing harmful electromagnetic radiation [10, 11]. Spinel ferrite (MFe_2O_4, M = Mn、Mg、Co、Cu、Zn、Ni、Fe etc.) exhibits adjustable saturation magnetization, excellent chemical stability, low real dielectric constant and high magnetic loss. Among these spinel ferrites, $CoFe_2O_4$ received particular attention due to their remarkable properties, which include a moderate saturation magnetization, excellent chemical stability, and high mechanical hardness [12]. On the basis of these characteristics, $CoFe_2O_4$ ferrite can be used as a powerful EMW adsorption material [13]. However, bulk magnet $CoFe_2O_4$ ferrite has disadvantages of high density, narrow bandwidth and large absorber thickness, which restricted their applications. In order to overcome these disadvantages and improve its adsorbing efficiency, one effective strategy is to immobilize ferrite nanoparticles (NPs) on high physical and chemical stability porous supports such as activated carbon [14], silica [15, 16] and grapheme [17, 18], which realized to wide absorbing band (below -10 dB), lightweight, corrosion resistance and high temperature resistance [3, 19-21].

Diatomite is a low-cost silicate mineral composed by silica microfossils of aquatic algae with high permeability and porous structure that possesses the properties of large surface area, small particle size, and remarkable thermal stability [22, 23]. Therefore, diatomite is one of the most promising supports for dielectric materials [9, 24], which explored for preparation of EMW adsorbing nanocomposite. It has technical challenges for general utilization of the coal-derived diatomite due to its high contents of organic matters and iron in diatomite industrial of China. Thus, the large-scale sustainable utilization of coral-derived diatomite as a porous support for preparation of EMW adsorbing materials was taken into consideration. In the presented work, the $CoFe_2O_4$/diatomite nanocomposite for EMW adsorbing was prepared by citric acid-nitrate sol-gel auto-combustion method using coal-derived diatomite as support. The electromagnetic properties of the as-prepared nanocomposites were studied in the frequency range of 0~18GHz.

2. Materials and methods

2.1 Materials

The experimental used diatomite is the purified from the Xianfeng coal mine of China. $CoCl_2.6H_2O$ of analysis grade was purchased from the pharmaceutical group of chemical reagents; $FeCl_3·6H_2O$, PVP, NaOH, and anhydrous ethanol were obtained from Chengdu Kelon Chemical Reagent company. All other chemicals or reagents were used without further purification.

2.2 Preparation of $CoFe_2O_4$/diatomite nanocomposite

2.2.1 Purification of diatomite

Generally, 250 g of diatomite was added into water to prepare aqueous suspension with water-diatomite ratio of about 20:1 (water depth: 40 cm). Then, the upper aqueous layer of 5 cm was taken out after stirring at a suitable speed (300 rpm) for 30 min. The remaining sample was centrifuged to obtain pellets of purified diatomite. The wetly pellets of purified diatomite was dried by common muffle furnace at 70 °C for experiments.

2.2.2 Preparation of $CoFe_2O_4$ NPs

For sintering was chosen based on the SiO_2-Al_2O_3 phase diagram [17], waiting for the following phase transitions: 450 °C – kaolinite–metakaolinite; 575 °C.

2.2.3 Preparation of nanocomposite

The purified diatomite was added into above mentioned first preparation process of $CoFe_2O_4$ NPs for preparation of suspension with various ratios. The as-prepared samples after auto-combustion process was homogenous dispersed into ethanol, and then ultrasonic treated 20 min and shaken at room temperature for 5h. The as-prepared samples were finally dried in a vacuum oven at room temperature overnight for characterization. Finally, the nanocomposite samples were calcined at different temperatures for 2 h in muffle furnace.

2.3 Characterization

The mineral phase characterization was carried out using X'Pert Pro X-ray diffractometer (XRD) from PA Nalytical, Netherlands. The ULTRA55 field emission scanning electron microscopy (FE-SEM) and Libra 200FE-type transmission electron microscopy (TEM) were used to observe the morphological characteristics. The magnetic characterizations were carried out using the BKT-4500Z high precision vibration sample magnetometer of Beijing Xinke GaoShan Technology Co., Ltd. An Agilent N5230C microwave network analyzer was used to analyze the microwave absorption characteristics of the material.

3. Results and discussions

3.1 Morphological observations

The FE-SEM and TEM were used for characterizing the morphology of samples. Micrographs show the formation of spherical $CoFe_2O_4$ NPs with average particle size of 40 nm (*Fig. 1a, 1e*). As shown in *Figures 1b* and *1f*, the distinctive porous structures of the diatomite were occupied by $CoFe_2O_4$NPs. The elemental components of $CoFe_2O_4$ NPs and $CoFe_2O_4$/diatomite nanocomposite (DCNC) were identified by EDX analysis (*Fig. 1c, 1d*). The EDX patterns qualitative confirmed the presence of Co, Fe and O in the DCNC.

3.2 XRD characterization

The XRD characteristics of $CoFe_2O_4$ NPs, DCNC and diatomite are show in *Fig. 2*. The diffraction peaks appeared at Bragg angles 2θ~18.3°, 30.1°, 35.4°, 37.1°, 43.1°, 53.4°,57.0°

and 62.6° corresponding to (111), (220), (311), (222), (400), (422), (511) and (440) planes of $CoFe_2O_4$, respectively with a=b=c=8.377, by which confirmed the formation of cubic spinel structure. The natural diatomite is in the amorphous form without showing crystalline peaks. The diffraction peaks show small amount of impurities of magnetite Fe_3O_4 and Quartz. The XRD pattern of CDNC shows that $CoFe_2O_4$ is successfully compounded with diatomite.

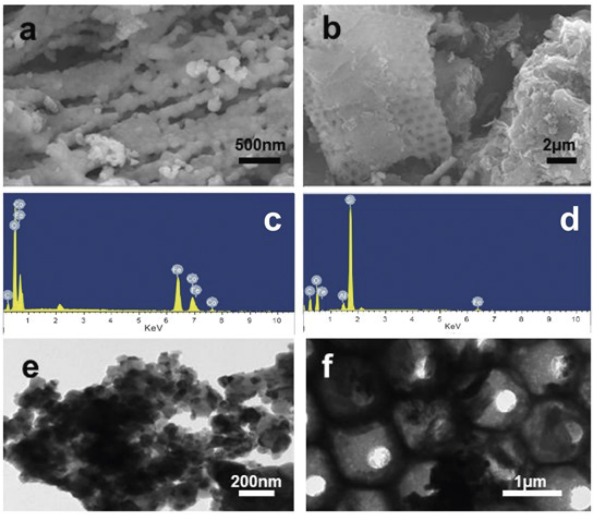

1. ábra FE-SEM EDX és TEM képekkel a CoFe2O4 NP-k és a CoFe2O4 NP-k DCNC-vel, a diatomit aránya 1: 10. CoFe2O4 NP (a, e,), DCNC (b, f). FESEM képek (a, b), FESEM-EDX a CoFe2O4 NP-ról (c), DCNC (d). TEM képek (e, f)

Fig. 1 FE-SEM with EDX and TEM images of $CoFe_2O_4$ NPs and DCNC with $CoFe_2O_4$ NPs to diatomite ratio of 1 to 10. $CoFe_2O_4$ NPs (a, e,), DCNC (b, f). FESEM images (a, b), FESEM-EDX patterns of $CoFe_2O_4$ NPs (c), DCNC (d). TEM images (e, f)

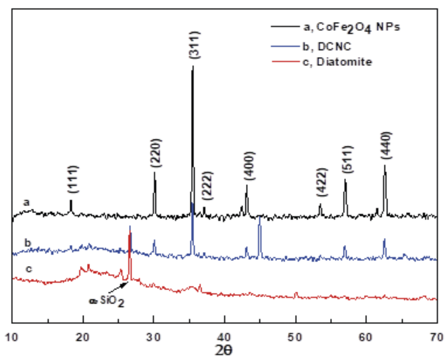

2. ábra A CoFe2O4NP-k, a diatomit és a DCNC XRD mintái, a CoFe2O4 NP-k 1-10 közötti diatomit arányokkal

Fig. 2 XRD patterns of $CoFe_2O_4$NPs, diatomite and DCNC with $CoFe_2O_4$ NPs to diatomite ratios of 1 to 10

3.3 Magnetic properties

$CoFe_2O_4$NPs is a kind of widely used magnetic nanomaterial with large ferromagnetic anisotropy constants. Its magnetic properties originated from the magnetic coupling interaction between Co^{2+} and Fe^{3+} ions through oxygen atoms [25, 26]. The magnetic hysteresis loops of all samples were measured by VSMat room temperature (*Fig. 3*). Magnetic parameters of $CoFe_2O_4$NPs and DCNC such as coercivity (Hc), saturation magnetization (Ms), retentivity and Remanence ratio (Mr/Ms) are presented in *Table 1*.

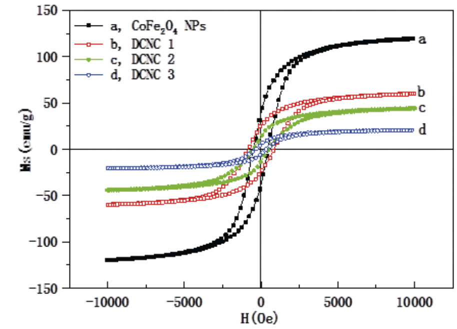

3. ábra A CoFe2O4 NP és DCNC mágnesezési görbéi. DCNC 1 és DCNC 3 CoFe2O4NP-kkel, a diatomit aránya 1:2, 1:5, illetve 1:10 között

Fig. 3 Magnetization curves of $CoFe_2O_4$ NPs and DCNC. DCNC 1 to DCNC 3 with $CoFe_2O_4$NPs to diatomite ratios of1 to 2, 1 to 5 and 1 to 10, respectively

Samples	Coercivity Hc (Oe)	Saturation magnetization Ms (emu.g^{-1})	Retentivity Mr (emu.g^{-1})	Rema-nenceratio Mr/Ms
$CoFe_2O_4$ NPs	837.07	96.5	49.9	0.52
DCNC 1	262.07	53.43	10.94	0.2
DCNC 2	148.21	43.39	6.04	0.14
DCNC 3	403.07	32.61	9.08	0.28

1. táblázat VSM-rel mért mágneses paraméterek CoFe2O4 NP-k, DCNC 1 és DCNC 3, CoFe2O4NP-k, diatomit arányaránya 1:2, 1: 5, illetve 1:10 között

Table 1 Magnetic parameters measured from VSM for $CoFe_2O_4$ NPs, DCNC 1 to DCNC 3 with $CoFe_2O_4$NPs to diatomite ratios of 1 to 2, 1 to 5 and 1 to 10, respectively

The hysteresis graphs for $CoFe_2O_4$ NPs and DCNC are typical of the soft magnetic material. $CoFe_2O_4$ NPs exhibits significant ferromagnetic behavior with Hc of 837.07Oe, Ms of 96.5 emu·g^{-1}, Mr of 49.9 and Mr/Ms of 0.52. It seems that existing strong ferromagnetic coupling among $CoFe_2O_4$ NPs, in which them ferromagnetically coupled together and behaving as magnetic nanochains rather than as individual NP [17]. As shown in *Fig. 3*, it is clear that the saturation magnetization of DCNC is much lower than the corresponding value of $CoFe_2O_4$ NPs. Lower saturation magnetization is contributed to the addition of non-magnetic diatomite to $CoFe_2O_4$ NPs. Therefore, from the aspect of engineering application, the magnetic properties of DCNC can be adjusted to meet the requirement of actual design by changing the compositions between diatomite and $CoFe_2O_4$ NPs.

3.4 Dielectric properties

The microwave dielectric properties of $CoFe_2O_4$ NPs and DCNC were measured at frequencies (0-18 GHz) by the microwave network analyzer. The electromagnetic properties are mainly characterized by two basic parameters[4, 27]as described by Eq.(1) and Eq.(2):

Complex permittivity, $\varepsilon_r = \varepsilon' + i\varepsilon''$ (1)

Complex magnetic permeability, $\mu_r = \mu' + i\mu''$ (2)

Where ε′ and ε″ are the real part or dielectric constant and imaginary part or dielectric loss of the complex dielectric permittivity. Where μ′ and μ″ are the real magnetic permeability and magnetic loss.

In addition, the dielectric loss tangent (tan δ) characterizes the dielectric loss of a dielectric material after applying an electric field. Where δ is dielectric loss angle. The electric loss tangent is determined by the complex permittivity:

$$\tan \delta_E = \frac{\varepsilon''}{\varepsilon'} \quad (3)$$

The magnetic loss tangent is determined by the complex permeability:

$$\tan \delta_M = \frac{\mu''}{\mu'} \quad (4)$$

3.4.1 Dielectric properties

It is well known that the dielectric constant is the expression of the polarization capacity of the material. Dipoles, interfaces, ions and electron polarization favor dielectric loss. At lower frequencies, dipole and interfacial polarization are important for dielectric loss. However, ion and electron polarization make a most significant contribution to the dielectric loss at higher frequency[28]. Polarization and variation of dielectric constant in $CoFe_2O_4$ and its complexes may be related to changes of Fe^{2+} and Fe^{3+} concentrations [29]. Moreover, the dielectric constant of $CoFe_2O_4$ and its complexes depends on the amount of Fe^{2+} in the microwave frequency because they are susceptible to polarization than Fe^{3+} [30].

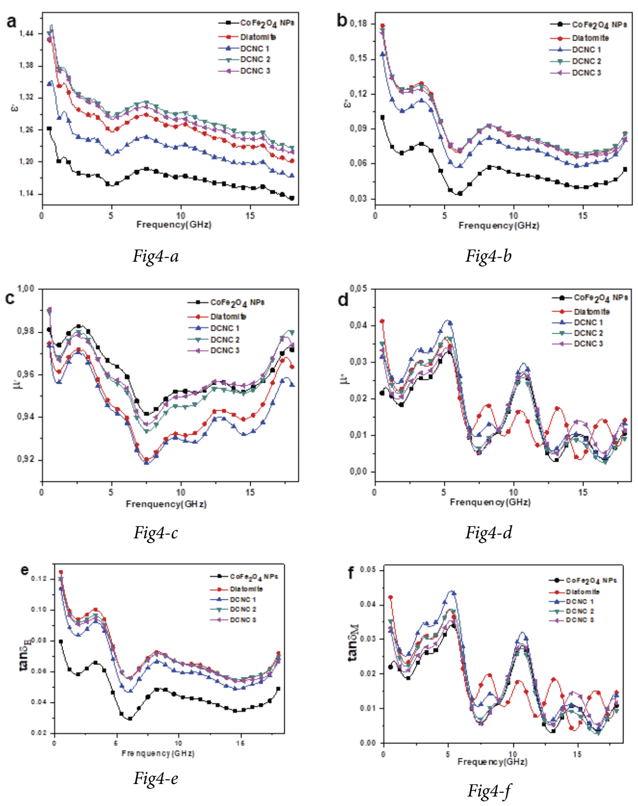

4. ábra A CoFe2O4 NP-k, a diatomit és a DCNC dielektromos tulajdonságai. DCNC 1 és DCNC 3 CoFe2O4 NP-k, a diatomit aránya 1:2, 1:5, illetve 1:10 között. Komplex permittivitás (ε, a, b), komplex permeabilitás (μ, c, d) és veszteségtangens (tanδ, e, f). Az ε (ε', a) valódi része, az ε (ε ", b) képzetes része. M (μ', c) valódi része, μ (μ", d) képzetes része. Elektromos veszteségtangens (tanδE, e), mágneses veszteségtangens (tanδM, f)

Fig. 4 Dielectric properties of $CoFe_2O_4$ NPs, diatomite and DCNC. DCNC 1 to DCNC 3 with $CoFe_2O_4$ NPs to diatomite ratios of 1 to 2, 1 to 5 and 1 to 10, respectively. Complex permittivity (ε, a, b), complex permeability (μ, c, d) and loss tangent (tanδ, e, f). Real part of ε (ε', a), imaginary part of ε (ε", b). Real part of μ (μ', c), imaginary part of μ (μ", d). Electric loss tangent ($\tan\delta_E$, e), magnetic loss tangent ($\tan\delta_M$, f)

The dielectric properties of $CoFe_2O_4$ NPs, diatomite and DCNC are shown in *Fig. 4* in the frequency range of 2~18GHz. The ε' of the samples always show a rapid decline and then a small increase, and finally a downward trend. ε" appears to fall and then rise and then fall again, finally in rising trend. At 4~6Hz, 7~9Hz *Fig. 4a* and *Fig. 4b* appear more obvious dielectric resonance peak. The values of ε', ε" in single $CoFe_2O_4$ are the smallest in the range of 2~18Hz. The value of ε' fluctuates between 1.26~1.13 and the value of ε" fluctuates in the range of 0.09~0.18. With the decrease in the mixing ratio of $CoFe_2O_4$ and diatomite, the values of ε', ε" have been significantly improved. When the ratio of $CoFe_2O_4$ to diatomite is 1:5, the values of ε', ε" are the largest and the best. The maximum values of ε', ε" are 1.47 and 0.18 respectively, and the minimum values are about 1.23 and 0.09 respectively. The peaks in the range of 4~6Hz are about 1.29 and 0.075 respectively, and the peaks in 7~9Hz are about 1.32 and 0.1. Significant relaxation peaks appeared at around 6 GHz and 15 GHz, indicating that there is dielectric relaxation in both $CoFe_2O_4$ NPsand composites [31] and the polarization is strong. But only when $CoFe_2O_4$ and diatomite ratio of 1:5 and 1:10, The values of ε', ε" are greater than a single diatomite and the effect is better after compositing. Although the composite of 1:10 is relatively smaller than that of 1:5, it is relatively close to that of 1:5. The maximum value of ε' is about 1.44 and the minimum value is about 1.22 when the ratio of $CoFe_2O_4$ to diatomite is 1:10. And its peaks in 4~6Hz and 7~9Hz are about 1.29 and 1.31 respectively. Its value of ε" is almost the same to the value of 1:5, so it is more economical in practical application. And when $CoFe_2O_4$ and diatomite ratio is 1:2, the values of ε', ε" are between single $CoFe_2O_4$ and single diatomite. Thus, the effect is general. The loss tangent represents the loss of the microwave absorbing material and supports the dominant contribution of conductivity to dielectric loss. It can be seen from the *Fig. 4e* that the value of a single diatomite is the largest and the value of single $CoFe_2O_4$ is the smallest, which is mainly because diatomite is a dielectric loss material and $CoFe_2O_4$ is electromagnetic loss material. As the ratio of $CoFe_2O_4$ to diatomite decreases, the loss tangent is also reduced.

3.4.2 Permeability properties

In the range of 2~18Hz, the values of μ' of each sample shows a trend of decreasing at first and then rising, and fluctuating in a small range. The value of μ" has a more complex change with a greater degree fluctuating. The value of μ' of a single $CoFe_2O_4$ is the largest in the range of 2~18Hz and the maximum is about 0.045, which is close to the ratio of $CoFe_2O_4$ to diatomite at 1:10. However, as the ratio of $CoFe_2O_4$ to diatomite increases, the value of μ' decreases at the same frequency. When the ratio of $CoFe_2O_4$ to diatomite is 1:2, the value of μ' is the smallest in the range of 2~18Hz and the minimum is about 0.92. The single diatomite is slightly larger than it. In addition, the value of μ" is the largest in the low frequency range whose maximum is about 0.045 but the single diatomite is the smallest and its minimum is about 0.015. In the high frequency range, the volatility is more complicated. The single diatomite is the largest in 12~14Hz and 16~18Hz and the peaks are about 0.023 and 0.015 respectively. Moreover, in 14~16Hz, the largest value is 0.015 when the ratio of $CoFe_2O_4$ to diatomite is 1:10. It can be seen from *Fig. 4d* that the magnetic permeability fluctuates greatly with frequency, and multiple resonance peaks appear, indicating the presence of ferromagnetic resonance behavior [32]. Dues to the influence of $CoFe_2O_4$ spinel structure on the anisotropy field, the magnetic field anisotropy causes a large change in magnetic permeability. The main source is that the unpaired electrons in the ferromagnetic medium use magnetic materials to absorb energy from the microwave magnetic field and cause magnetic energy loss. According to the analysis of magnetic loss tangent, in the low frequency range, the loss is the largest when the ratio of $CoFe_2O_4$ to diatomite is 1:2 and the performance is closer when the ratio of $CoFe_2O_4$ to diatomite is 1:5 and 1:10. In the High-frequency range, the ratio of $CoFe_2O_4$ to diatomite is 1:10 better than 1:5, and the loss angle tangent is greater.

In general, when the dielectric and magnetic properties of the composites are matched with each other, the microwave absorption effect will be better. Considering the economic rationality and the absorbing effect, when the ratio of $CoFe_2O_4$ to diatomite is 1:10, the dielectric dissipation effect of diatomite and the magnetic dissipation effect of $CoFe_2O_4$ NPs can be combined to achieve the best absorbing properties.

3.4.3 Microwave absorption properties

As shown in *Fig. 5*, the microwave absorption performances of the samples are basically the same, which have the best absorption effect when nearing 11 GHz. This phenomenon is consistent with the above analysis of the permeability. The porous structure of the diatomite as the matrix causes the electromagnetic wave traveling path to cause the formation of multiple internal reflections and multiple scattering, which significantly enhances the attenuation capability, thereby contributing to the enhancement of microwave absorption performance [33]. When the ratio of $CoFe_2O_4$ to diatomite is 1:2, the composite has the best absorbing effect. When the ratio of $CoFe_2O_4$ to diatomite is 1:10 and 1:5, the wave absorbing performance is the second. The peak is about -9dB in 4~6Hz. The range of <-10Hz is between 10Hz and 12Hz and the maximum reflection loss is about -12dB. In addition, when the ratio of $CoFe_2O_4$ to diatomite is 1:10, the composite has the best absorbing effect whose maximum reflection loss is about -9dB ranging from 12 to 18Hz, while the maximum reflection loss of other materials is only about -7Hz. As shown in *Table 2*, it reflects the maximum reflectivity loss for each material. From the economic point of view, when the ratio of $CoFe_2O_4$ to diatomite is 1:10, the absorbing performance is close to that of $CoFe_2O_4$ and diatomite of 1:2 in the low frequency range. Moreover, in the high frequency range, the composite of 1:10 has the best absorption effect.

Therefore, the composite of 1:10 is most conducive to the promotion. It is worth noting that $CoFe_2O_4$ and its complex have two secondary absorption peaks near the 5 GHz and 15 GHz frequencies, which correspond to the minimum value of the sample loss tangent rather than the sub-peak corresponding to the loss tangent. The absorption peak has moved. In a word, the absorbing ability of the material is not only closely related to its permeability, but also has a significant relationship with the thickness of the absorbing plate, which will result in the left and right offset of peak positions of absorption peaks and values of loss tangent. Therefore, the wide peak value of the loss tangent will be of great importance to the expansion of absorbing capacity, so that the material can meet the requirements of multi-band and various thicknesses.

Sample	Maximum reflectivity loss/dB	The corresponding frequency/Hz
$CoFe_2O_4$ NPs	10.73	10.83
Diatomite	8.42	18
DCNC 1	12.04	10.74
DCNC 2	10.59	10.74
DCNC 3	11.17	10.83

2. táblázat A CoFe2O4 NP-k, a diatomit és a DCNC maximális reflexiós vesztesége. DCNC 1 és DCNC 3 CoFe2O4NP-k, a diatomit aránya 1:2, 1:5, illetve 1:10 között

Table 2 The maximum reflectivity loss of $CoFe_2O_4$ NPs, diatomite and DCNC. DCNC 1 to DCNC 3 with $CoFe_2O_4$NPs to diatomite ratios of 1 to 2, 1 to 5 and 1 to 10, respectively

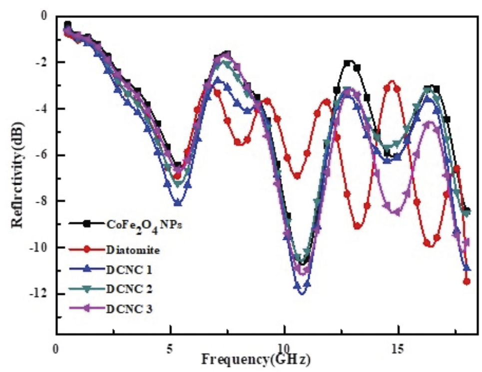

5. ábra A CoFe2O4 NP-k, a diatomit és a DCNC mikrohullámú abszorpciós tulajdonságai. DCNC 1 és DCNC 3 CoFe2O4NP-kkel, a diatomit aránya 1: 2, 1:5, illetve 1:10 között

Fig. 5 Microwave absorption properties of $CoFe_2O_4$ NPs, diatomite and DCNC. DCNC 1 to DCNC 3 with $CoFe_2O_4$NPs to diatomite ratios of1 to 2, 1 to 5 and 1 to 10, respectively

4. Conclusions

In summary, the DCNC of $CoFe_2O_4$/diatomite were fabricated via citric acid-nitrate sol-gel auto-combustion method. The FE-SEM and TEM observations confirmed that the magnetic NPs were uniformly dispersed in the surface and porous structure of diatomite to form stable DCNC. Magnetic measurements show that all samples are ferromagnetic, and that the Co^{2+} occupies the octahedral (B) site, will result in a reduction in the A-O-B super exchange interaction and a total of the magnetic properties of Fe^{3+} ions reduce. The microwave dielectric properties of the DCNC show that the dielectric and magnetic properties of the composites are optimized. The optimized best absorption performance of DCNC with ratio of $CoFe_2O_4$ to diatomite is 1:10 considering the economic rationality and the absorbing performances. In generally, our study shows a promising way for construction of diatomite-based functional nanomaterials.

5. Acknowledgements

This work was supported by the National Natural Science Foundation of China (NSFC, Nos. 42011530085, 41672039), Russian Foundation for Basic Research (RFBR, No. 20-55-53019), the Sichuan Science and Technology Program (2019JDJQ0056), and the Longshan Academic Talent Research Support Program of the Southwest University of Science and Technology (18LZX405).

References

[1] Cao, S. – Ding, Y. – Yang, M. – Pan, H.: Lightweight and nitrogen-doped graphene nanoribbons with tunable hierarchical structure for high performance electromagnetic wave absorption. Ceramics International, 2018; 44(16): 20259-20266.

[2] Deniz, Ö. G. – Kıvrak, E. G. – Kaplan, A. A. – Altunkaynak, B. Z.: Effects of folic acid on rat kidney exposed to 900 MHz electromagnetic radiation. Journal of Microscopy & Ultrastructure, 2017; 5(4): 198-205.

[3] Gandhi, N. – Singh, K. – Ohlan, A. – Singh, D. P.: Thermal, dielectric and microwave absorption properties of polyaniline-$CoFe_2O_4$ nanocomposites. Composites Science & Technology, 2011; 71(15): 1754-1760.

[4] Moradmard, H. – Shayesteh, S. F. – Tohidi, P. – Abbas, Z:. Structural, magnetic and dielectric properties of magnesium doped nickel ferrite NPs. Journal of Alloys and Compounds, 2015; 650: 116-122.

[5] Lenin, N. – Sakthipandi, K. – Kanna, R. R. – Rajkumar, G.: Electrical, magnetic and structural properties of polymer-blended lanthanum-added nickel nano-ferrites. Ceramics International, 2018; 44(17): 21866-21873.

[6] Wen, B. – Cao, M. – Lu, M. – Cao, W.: Reduced graphene oxides: light-weight and high-efficiency electromagnetic interference shielding at elevated temperatures. Advanced Materials, 2014; 26(21): 3484-3489.

[7] Yuan, L. M. – Xu, Y. G. – Dai, F. – Liao, Y.: The microwave properties of composites including lightweight core-shell ellipsoids. Journal of Magnetism and Magnetic Materials, 2016; 419: 494-499.

[8] Feng, A. – Jia, Z. – Zhao, Y. – Lv, H.: Development of Fe/Fe_3O_4@C composite with excellent electromagnetic absorption performance. Journal of Alloys and Compounds, 2018; 745: 547-554.

[9] Yan, Z. Q. – Cai, J. – Xu, Y. G. – Zhang, D. Y.: Microwave absorption property of the diatomite coated by Fe-CoNiP films. Applied Surface Science, 2015; 346: 77-83.

[10] O'Handley, R. C.: Modern Magnetic Materials: Principles and Applications. 2000.

[11] Decurtins, S.: Magnetic Materials. Fundamentals and Device Applications. Von Nicola Spaldin. Angewandte Chemie International Edition, 2003; 42(47): 5791-5791.

[12] Zhao, D. – Wu, X. – Guan, H. – Han, E.: Study on supercritical hydrothermal synthesis of $CoFe_2O_4$ NPs. Journal of Supercritical Fluids, 2007; 42(2): 226-233.

[13] Zhang, S. – Jiao, Q. – Zhao, Y. – Li, H.: Preparation of rugby-shaped $CoFe_2O_4$ particles and their microwave absorbing properties. Journal of Materials Chemistry A, 2014; 2(42): Accepted Manuscript, 18033-18039.

[14] Wang, L. – Guan, Y. – Qiu, X. – Zhu, H.: Efficient ferrite/Co/porous carbon microwave absorbing material based on ferrite@metal–organic framework. Chemical Engineering Journal, 2017; 326: 945-955.

[15] Yan, X. – Chen, J. – Xue, Q. – Miele, P.: Synthesis and magnetic properties of $CoFe_2O_4$ NPs confined within mesoporous silica. Microporous & Mesoporous Materials, 2010; 135(1): 137-142.

[16] Bagheri, M. – Bahrevar, M. A. – Beitollahi, A.: Synthesis of mesoporous magnesium ferrite ($MgFe_2O_4$) using porous silica templates. Ceramics International, 2015; 41(9, Part B): 11618-11624.

[17] Liu, P. – Huang, Y. – Zhang, X.: Synthesis, characterization and excellent electromagnetic wave absorption properties of graphene@$CoFe_2O_4$ @ polyaniline nanocomposites. Synthetic Metals, 2015; 201: 76-81.

[18] Yang, H. – Ye, T. – Lin, Y. – Liu, M.: Preparation and microwave absorption property of graphene/$BaFe_{12}O_{19}$/$CoFe_2O_4$ nanocomposite. Applied Surface Science, 2015; 357(3): 1289-1293.

[19] Sun, Z. – Yao, G. – Liu, M. – Zheng, S.: In situ synthesis of magnetic $MnFe_2O_4$/diatomite nanocomposite adsorbent and its efficient removal of cationic dyes. Journal of the Taiwan Institute of Chemical Engineers, 2017; 71: 501-509.

[20] Fu, W. – Liu, S. – Fan, W. – Yang, H.: Hollow glass microspheres coated with $CoFe_2O_4$ and its microwave absorption property. Journal of Magnetism & Magnetic Materials, 2007; 316(1): 54-58.

[21] Shen, W. – Ren, B. – Cai, K. – Song, Y-f.: Synthesis of nonstoichiometric $Co_{0.8}Fe_{2.2}O_4$/reduced graphene oxide (rGO) nanocomposites and their excellent electromagnetic wave absorption property. Journal of Alloys and Compounds, 2019; 774: 997-1008.

[22] Zha, Y. – Zhou, Z. – He, H. – Wang, T.: Nanoscale zero-valent iron incorporated with nanomagnetic diatomite for catalytic degradation of methylene blue in heterogeneous Fenton system. Water Science and Technology, 2016; 73(11): 2815-2823.

[23] Yusan, S. – Korzhynbayeva, K. – Aytas, S. – Tazhibayeva, S.: Preparation and investigation of structural properties of magnetic diatomite nanocomposites formed with different iron content. Journal of Alloys and Compounds, 2014; 608: 8-13.

[24] Dehestaniathar, S. – Khajelakzay, M. – Ramezani-Farani, M. – Ijadpanah-Saravi, H.: Modified diatomite-supported CuO-TiO_2 composite: Preparation, characterization and catalytic CO oxidation. Journal of the Taiwan Institute of Chemical Engineers, 2016; 58: 252-258.

[25] Ayyappan, S. – Philip, J. – Raj, B.: Effect of Digestion Time on Size and Magnetic Properties of Spinel $CoFe_2O_4$ NPs. Journal of Physical Chemistry C, 2009; 113(2): 590-596.

[26] Manova, E. – Kunev, B. – Paneva, D. – Mitov, I.: Mechano-Synthesis, Characterization, and Magnetic Properties of NPs of Cobalt Ferrite, $CoFe_2O_4$. Chemistry of Materials, 2004; 16(26): 5689-5696.

[27] Yusoff, A. N. – Abdullah, M. H. – Ahmad, S. H. – Jusoh, S. F.: Electromagnetic and absorption properties of some microwave absorbers. Journal of Applied Physics, 2002; 92(2): 876-882.

[28] Kumar, A. – Sharma, P. – Varshney, D.: Structural, vibrational and dielectric study of Ni doped spinel Co ferrites: Co_1–$xNi_xFe_2O_4$ (x =0.0, 0.5, 1.0). Ceramics International, 2014; 40(8): 12855-12860.

[29] Rezlescu, N. – Rezlescu, E.: Dielectric properties of copper containing ferrites. Physica Status Solidi, 2010; 23(2): 575-582.

[30] Verma, A. – Saxena, A. K. – Dube, D. C.: Microwave permittivity and permeability of ferrite–polymer thick films. Journal of Magnetism & Magnetic Materials, 2003; 263(1): 228-234.

[31] Liu, Z. – Xu, G. – Zhang, M. – Xiong, K.: Synthesis of $CoFe_2O_4$/RGO nanocomposites by click chemistry and electromagnetic wave absorption properties. Journal of Materials Science Materials in Electronics, 2016; 27(9): 1-8.

[32] Liu, J. – Cao, M. S. – Luo, Q. – Shi, H. L.: Electromagnetic Property and Tunable Microwave Absorption of 3D Nets from Nickel Chains at Elevated Temperature. Acs Applied Materials & Interfaces, 2016; 8(34): 22615.

[33] Jiang, L. – Liu, L. – Xiao, S. – Chen, J.: Preparation of a novel manganese oxide-modified diatomite and its aniline removal mechanism from solution. Chemical Engineering Journal, 2016; 284: 609-619.

Ref.:

Huang, Haodong – **He**, Meng – **Kotova**, Olga B. – **Golubev**, Yevgeny – **Dong**, Faqin – **Gömze**, László A. – **Kurovics**, Emese – **Lv**, Rui – **Sun**, Shiyong: *Preparation and electromagnetic microwave adsorption performances of porous nanocomposite self-assembled by $CoFe_2O_4$ nanoparticles and diatomite*
Építőanyag – Journal of Silicate Based and Composite Materials, Vol. 72, No. 4 (2020), 124–129. p.
https://doi.org/10.14382/epitoanyag-jsbcm.2020.20

Effect of composition and sintering temperature on thermal properties of zeolite-alumina composite materials

Jamal-Eldin F. M. IBRAHIM ▪ Institute of Ceramics and Polymer Engineering, University of Miskolc, Hungary ▪ jamalfadoul@gmail.com
Dmitry A. SHUSHKOV ▪ Institute of Geology, FRC Komi Science Center, Ural Branch of the Russian Academy of Sciences, Russian Federation ▪ dashushkov@geo.komisc.ru
Emese KUROVICS ▪ Institute of Ceramics and Polymer Engineering, University of Miskolc, Hungary ▪ fememese@uni-miskolc.hu
Mohammed TIHTIH ▪ Institute of Ceramics and Polymer Engineering, University of Miskolc, Hungary ▪ medtihtih@gmail.com
Olga B. KOTOVA ▪ Institute of Geology, FRC Komi Science Center, Ural Branch of the Russian Academy of Sciences, Russian Federation ▪ kotova@geo.komisc.ru
Péter PALA ▪ Refratechnik Hungaria Ltd, Hungary
László A. GÖMZE ▪ Institute of Ceramics and Polymer Engineering, University of Miskolc, Hungary, IGREX Engineering Service Ltd ▪ femgomze@uni-miskolc.hu
Érkezett: 2020. 06. 30. ▪ Received: 30. 06. 2020. ▪ https://doi.org/10.14382/epitoanyag-jsbcm.2020.21

Abstract

This research work provides a technical description of the utilization of natural zeolites in the synthesis of ceramic composite material using mechanical milling and reactive sintering technique. Two commercially available minerals (Natural zeolite from Mád in Tokaj region and MOTIM Al_2O_3) were used as starting raw materials, A comprehensive analysis has been conducted for the detailed characterization of raw materials as well as produced products, the analysis combines the mineralogical examination using X-ray diffraction (XRD) together with chemical constituent determination by (XRF) and thermoanalytical studies using (TG/DTA), heating electron microscope and thermal conductivity analyzer to determine the influence of sintering temperatures on the thermal properties of the produced zeolite-alumina composite materials. Based on the results obtained from XRD, XRF and TG/DTA, the authors have found a great connection between the composition, firing temperature and thermal properties of the produced ceramic samples.
Keywords: zeolite-alumina, composite materials, uniaxial compaction, thermal properties
Kulcsszavak: zeolit - alumínium-oxid, kompozit anyag, egytengelyű sajtolás, termikus tulajdonságok

Jamal-Eldin F. M. IBRAHIM
is a lecturer in the University of Bahri, Khartoum, Sudan, he graduated from University of Marmara, Istanbul, Turkey, Institute of Pure and Applied Sciences, Department of Metallurgical and Materials Engineering, for the time being, he is a PhD student in the University of Miskolc, Institute of Polymer and Ceramics Engineering, under supervision of Prof. L. A. Gömze.

Dmitry A. SHUSHKOV
is Researcher of Laboratory of Technology of Mineral Raw, Institute of Geology Komi SC UBRussian Academy of Sciences. Author and co-author of 2 patents and more than 40 scientific articles. Russian Mineralogical Society

Emese KUROVICS
is graduated from the University of Miskolc, Department of Ceramics and Silicate Engineering as a material engineer, where she continues her study as PhD student under supervision of Prof. L. A. Gömze.

Mohammed TIHTIH
Is a lecturer in the Sidi Mohamed Ben abdellah University, Morocco, he graduated from Faculty of sciences Dhar El Mahraz, Fez, Morocco, Department of Physics, for the time being, he is a PhD student in the University of Miskolc, Institute of Ceramics and Polymer Engineering, under supervision of Prof. L. A. Gömze

Olga B. KOTOVA
is Head of Laboratory of Technology of Mineral Raw, Institute of Geology Komi SC UB Russian Academy of Sciences. Author and co-author of 10 books, 4 patents and more than 200 scientific articles. President of ICAM-2019. The member of Science Council of Russian Mineralogical Society.

Péter PALA
Is a chemical engineer who finished his study at the University of Pannonia. He has been working in the ceramics industry since 2003, at present he is the managing director of Refratechnik Hungaria Ltd.

László A. GÖMZE
is establisher and professor of the Department of Ceramics and Silicate Engineering in the University of Miskolc, Hungary. He is author or co-author of 2 patents, 6 books and more than 300 scientific papers.

1. Introduction

Currently, ceramics materials both traditional and advance materials have attracted huge interest in research and industries [1-14]. Zeolites are a large group of naturally occurring minerals, normally consist of hydrated aluminosilicates of sodium, potassium, calcium, and barium which are formed from largely extending three-dimensional frameworks of $[SiO_4]^{4-}$ and $[AlO_4]^{5-}$ tetrahedra bonded from their corners with shared oxygen atoms (*Fig. 1*) [15] . Zeolite is characterized by their porous structures with large interconnected cavities that accommodate cations such as Na^+, K^+, Ca^{2+} and Mg^{2+} that neutralized the negatively charged framework [16,17]. Various structures (more than 200) are introduced for zeolites, in which 20% is considered as natural minerals and the reminders are synthetic materials. Zeolite which can be prepared in a high amount at relatively moderate temperatures is popular for large-scale applications. Therefore, high-alumina zeolites with large pore systems, for example, zeolites Linde type A (LTA) and zeolites Linde type X, are the most highly used zeolites in industries [15].

Large effort has lately been devoted to produce ceramic composite materials with enhanced properties using available and cost-effective materials. Natural zeolites are interesting candidates that can be used in the synthesis of many ceramic composites [18-23] due to their fascinating properties such as large surface area, high ions exchange capacity, high sorption capacity and their porous structure that can host secondary materials. Many applications for zeolite and zeolite-based materials have been introduced including building materials such as bricks, lightweight aggregate and additives for cement and concretes etc. Other technical applications of zeolite-based materials in many industries have also been reported for instance heterogeneous catalysis, sorbents and ion exchangers [24-25].

The ceramic forming techniques involve many processes such as pressing, extrusion, injection moulding, casting, sol-gel ect. The pressing technique is advantageous over other methods due to its low cost, simplicity and high productivity. All these production lines involve several steps, including, raw materials preparation, shaping techniques, drying method, sintering temperature and residence time. During the firing process which normally take places at a temperature ranging from 1/2 to 3/4 of the melting temperature of the ceramic raw materials [26]. The ceramic green bodies undergo a series of important changes, involving binder burnout, physico-chemical reactions (e.g. decomposition, oxidation), allotropic transformation, and sintering. These changes play a crucial role in the quality of the produced samples [27]. Due to the physicochemical reactions the sample raw materials are transformed into new complex compounds which govern the stability of the final ceramic products because of the change in volume of the system (increase or decrease). The densification due to the sintering has high influence in the physical and thermal properties of the ceramic products like porosity, density, and thermal conductivity, etc.

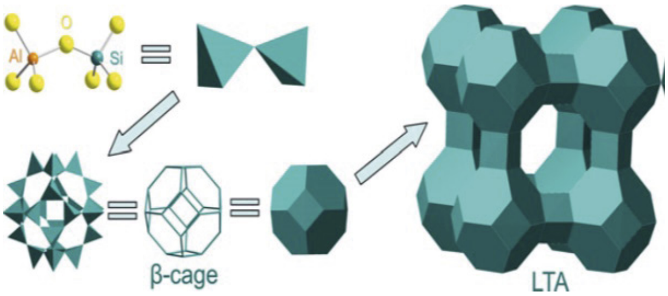

1. ábra A zeolitok sematikus felépítése SiO4 és AlO4 tetraéderekből és a zeolit egyszerűsített poliéderes szerkezetének ábrázolása [15]
Fig. 1 Schematic construction of zeolites from SiO_4 and AlO_4 tetrahedra and simplified polyhedra representation of a zeolite structure [15]

The goal of this paper is to investigate the effect of the change of sintering temperatures on thermal properties of zeolite-alumina composite materials. The natural zeolite is taken from Mád in Tokaj region which is a well-known area for a large deposit of natural zeolite, located on the north of Hungary as shown in *Fig. 2*.

2. ábra A természetes zeolit elhelyezkedése Mádban (Tokaji régió, Magyarország)
Fig. 2 Location of the natural zeolite in Mád (Tokaj region, Hungary)

2. Materials and experiments

2.1 Preparation methods

Natural zeolite from Mád (Tokaj region) and MOTIM Al_2O_3 powders were taken as starting raw materials. Five different compositions of zeolite and Al_2O_3 weight ratios were mixed in Retsch PM 400 planetary ball mill operated at the speed of 150 rpm for 15 minutes. The prepared powder mixtures are then compacted using a uniaxial compacting machine with a mechanical pressure of 100 MPa to produce cylindrical ceramic discs with a thickness of approximately 10 mm and a diameter of 25 mm. The produced ceramic compacts were fired at 1100 °C, 1150 °C, 1200 °C, 1250 °C and 1300 °C temperatures, using a programmable laboratory furnace with the heating rate of 60 °C/h and residence time of 3 h at the highest temperature. The samples of the sintered specimens are shown in *Fig. 3*.

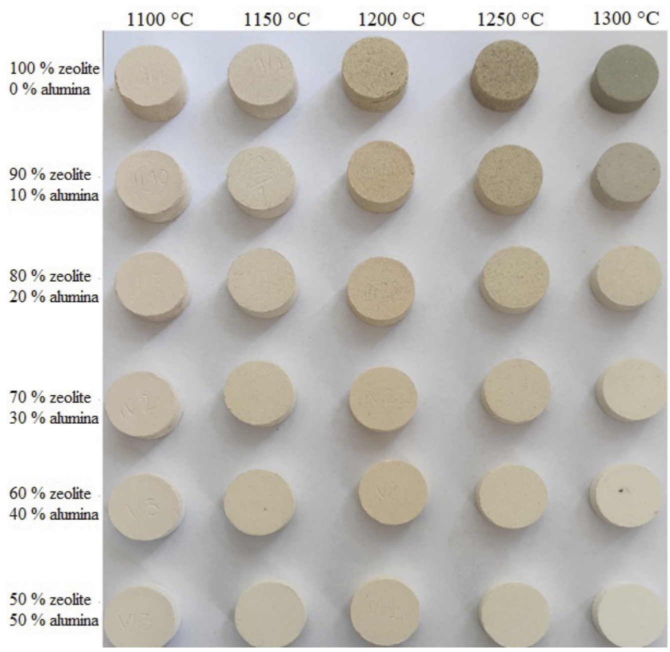

3. ábra Különböző összetételű minták, különböző hőmérsékleten szinterelve
Fig. 3 Samples with different composition sintered at different temperature

2.2 Characterization techniques

Phase identification of raw materials and the final product was done via XRD method using a Rigaku Miniflex II X-ray diffractometer, with CuKα radiation (λ= 1.54184 A). XRD patterns were scanned in step size of 0.01016° in a range of 2θ intervals of 0-70°. The effect of sintering temperature on the raw materials and prepared mixtures was also carried out using the heating microscope as well as the concurrent thermogravimetric analysis (TGA) and differential thermal analysis (DTA) methods which enable the persistent determination of the samples weight loss based on the temperature. The thermal conductivity of the prepared ceramics is performed via C-Therm TCi Thermal Conductivity Analyzer which applies the modified transient plane source (MTPS) technique in the determination of the thermal conductivity and effusivity of materials.

3. Results and discussions

3.1 XRD investigations

The XRD analysis of the raw materials (natural zeolite powder) from Mád (Tokaj region, Hungary) are confirmed to have many minerals phases together with zeolite (clinoptilolite) as shown in *Fig. 4*. *Table 1* shows the oxides and phases percentages of the natural zeolite in wt.% acquired from XRF and XRD tests. Silica (cristobalite) is found in the highest amount with a percentage of 50% while montmorillonite accounts for 30% and the other minerals represent 20% of the total amount.

Based on the composition of the oxides the overall amount of silica is found to be 82.92 wt.% and the reminders are other oxides like alumina, magnesia and sodium oxide.

Fig. 5 shows the XRD diffractogram of alumina from MOTIM. The XRD investigation reveals a complete match of the peaks which is an indication for the existence of alumina with single-phase (corundum).

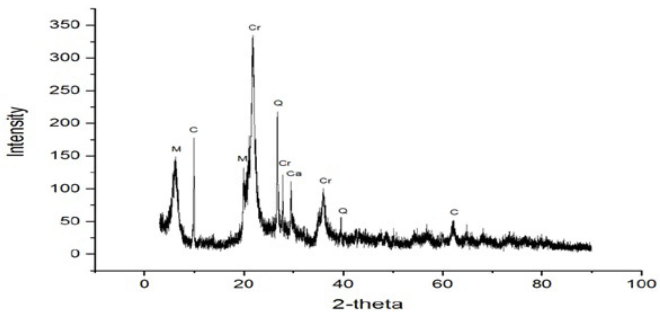

4. ábra A természetes zeolit minták XRD diffraktogramja (M: montmorillonit; C: klinoptilolit; Cr: cristobalite; Q: kvarc; Ca: kalcit)
Fig. 4 XRD diffractogram of the natural zeolite specimens (M: montmorillonite; C: clinoptilolite; Cr: cristobalite; Q: quartz; Ca: calcite)

	wt. %	CaO	SiO_2	Al_2O_3	MgO	Na_2O	CO_2	H_2O	Loss on ignition
Quartz	8.00		8.00						0.00
Cristobalite	50.00		50.00						0.00
Montmoril-lonite	30.00		19.13	4.06	3.21	0.74		2.87	2.87
Calcite	2.00	1.12					0. 88		0.88
Clinoptilolite	10.00		5.79	1.89		0.57		1.60	1.75
Total	100.00	1.12	82.92	5.95	3.21	1.31	0. 88	4.47	5.50

1. táblázat Az oxidok és az ásványi fázisok összetétele és tömegszázaléka
Table 1 The composition and weight percentage of the oxides and mineral phases

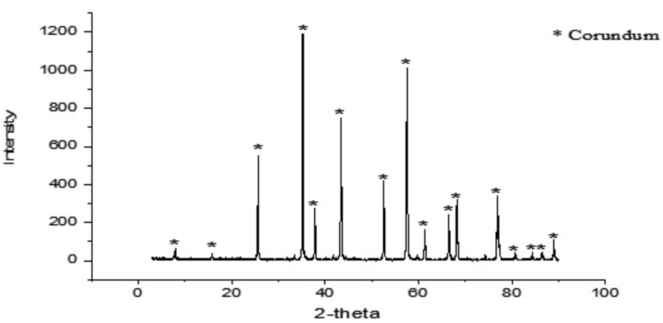

5. ábra Az alumínium-oxid XRD diffraktogramja
Fig. 5 XRD diffractogram of alumina

3.2 Thermal properties of raw materials

The thermal characteristics of naturally occurring zeolites vary remarkably from one type to another and highly govern their applications. Upon heating, zeolites in general tends to lose water (free and crystalline) and experience dehydration-accompanied volume shrinkage, which is completely or partially irreversible, especially when zeolites undergo modification in the tetrahedral structure.

TG/DTA curves of the ceramic raw materials with 90% zeolite and 10% alumina are shown in *Fig. 6*. Overall weight loss of approximately 8.4% was obtained at 1190 °C. Firstly, 2.01% decrease in the mass was observed in a temperature range of 40-102 °C which accounts to the removal of free water which normally exist in the zeolites surface, micropores and channels [26] Secondly, a weight loss of 3.74% was obtained in a temperature between 102 °C and 163,8 °C which could be attributed to the evaporation of the water in the closed pores and burning of the organic content. In the third steps and at the temperature between 163,8 °C-242.2 °C a weight loss of 4.57% was gained which could be due to the continuous burning of the low flammable materials (hydrocarbons). The largest weight loss was revealed at a temperature between 242 °C and 761 °C which ascribed to the evaporation of crystalline water. Small reaction was obtained at about 761-1190 °C which could be assigned to the decomposition of calcite and montmorillonite and/or formation of mullite and anorthite.

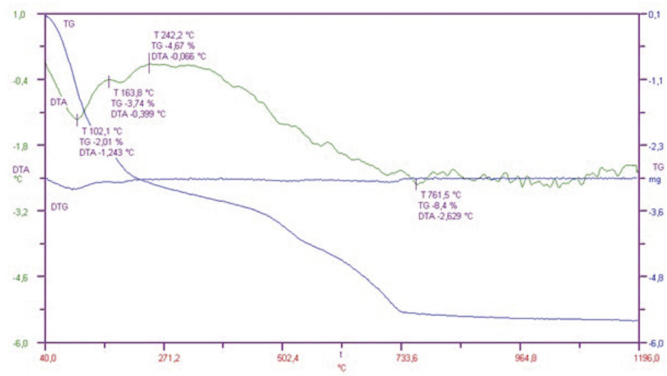

6. ábra 90% zeolit-10% alumínium-oxid por DTA, TG és DTG görbéi
Fig. 6 DTA, TG and DTG curves of 90% zeolite-10% alumina powder

The behavior of the ceramic mixtures under firing is examined using a Camar Elettronica heating microscope as shown in *Fig. 7*. Zeolite-alumina mixtures were stable up to 1358 °C, no melting was observed only sintering of the mixtures was noticed with 5% height shrinkage.

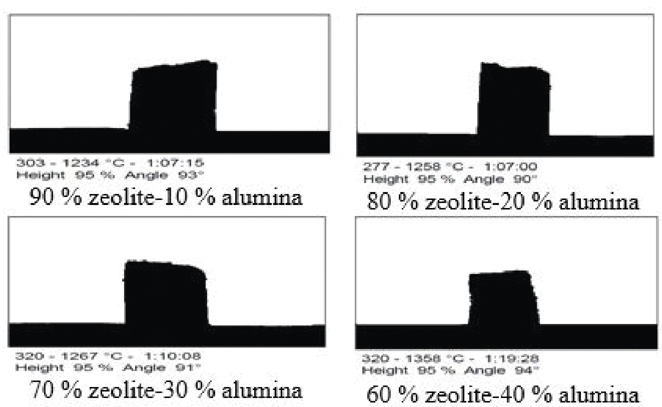

7. ábra A zeolit-alumínium-oxid keverékek különböző összetételű hevítőmikroszkópos képei
Fig. 7 Heating microscope images of different composition of zeolite-alumina mixtures

Natural zeolite from Mád (Tokaj region, Hungary) contains different minerals, therefore when mixed with alumina and fired, it undergoes various complex processes including dehydration of water followed by allotropic transformation (quartz to cristobalite), physicochemical reactions (formation of new mineral phase) and sintering and it can be clearly seen in *Fig. 3* which shows the change in colour and the volume shrinkage of the produced specimens based on the change in firing temperature. This could be a clue for the above-mentioned processes.

XRD of the sintered samples *Fig. 8* confirms the decomposition of montmorillonite and calcite, as well as the formation of mullite and anorthite at a temperature above 1000 °C, moreover, the amount of amorphous phase is increasing at higher sintering temperature. It is worth mentioning that in both cases, the firing of (natural zeolite and natural zeolite + alumina) leads to formation of mullite and anorthite but in case of firing zeolite-alumina mixture, larger amount of mullite and anorthite is expected to produce. Moreover, the volume shrinkage is increasing with increasing the firing temperature and hence the density is also increased.

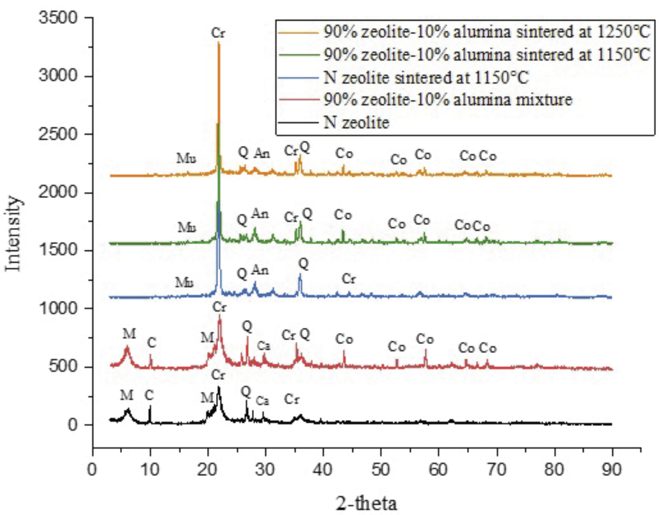

8. ábra A különböző hőmérsékleten szinterezett minták XRD diffraktogramja (M: montmorillonit, C: klinoptilolit, Cr: kristobalit Q: kvarc, Ca: kalcit, Mu: mullit, An: anortit, Co: korund)

Fig. 8 The XRD pattern of samples sintered at different temperatures (M: montmorillonite, C: clinoptilolite, Cr: cristobalite Q: quartz, Ca: calcite, Mu: mullite, An: anorthite, Co: corundum).

3.4 Thermal conductivity

The thermal conductivity of the prepared samples as a function of zeolite composition sintered at different temperatures (1100 °C, 1150 °C, 1200 °C, 1250 °C and 1300 °C) are shown in *Fig. 9*. Thermal conductivity of the samples tends to increase with increasing the sintering temperature due to the increase in density and reduction in porosity, the lowest thermal conductivity is found to be 0.3 W/mK achieved when 100% natural zeolite is sintered at 1100 °C. It can be noticed that increasing the alumina composition in the produced specimens tends to increase the thermal conductivity and this could be attributed to the formation of mullite and anorthite.

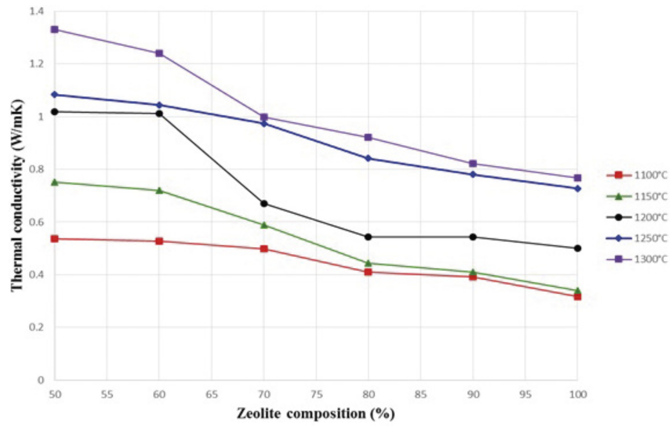

9. ábra A különböző hőmérsékleten szinterezett zeolit-alumínium-oxid minták hővezetőképessége

Fig. 9 The thermal conductivity of the zeolite-alumina samples sintered at different temperatures

4. Conclusions

Thermally-induced volume shrinkage and structural transformation were obtained due to the loss of free and combined water molecules by dehydration, decomposition of montmorillonite and calcite and formation of a new phases (mullite and anorthite) which firstly noticed by the change in the colour of the produced specimens and further confirmed by XRD, the formation of mullite and anorthite has resulted from the reaction of the added amount of alumina together with silica and the decomposed montmorillonite existing in the natural zeolite. All these processes lead to increase in the volume shrinkage of the prepared samples and hence increase the density and as a result, the thermal conductivity of the samples is also increased. The composition of the mixtures of the raw materials is found to has a large influence in the thermal conductivity and this could be resulted from the addition of alumina that induced the formation of mullite and anorthite at higher temperature.

Acknowledgments

The described article was carried out as part of the EFOP-3.6.1-16-00011 "Younger and Renewing University – Innovative Knowledge City – institutional development of the University of Miskolc aiming at intelligent specialisation" project implemented in the framework of the Szechenyi 2020 program. The realization of this project is supported by the European Union, co-financed by the European Social Fund. We would like to express our massive thank to Mr. Tibor MÁTYÁS from Geoproduct-Kružlov for his help and cooperation

References

[1] Gömze, László A., et al. "Conventional Brick Clays as a Challenge of Materials Science–New Explanation of Drying Sensitivities." IOP Conference Series: Materials Science and Engineering. Vol. 613. No. 1. IOP Publishing, 2019. https://doi.org/10.1088/1757-899X/613/1/012005

[2] Kurovics, Emese, et al. "Preparation of particle-reinforced mullite composite ceramic materials using kaolin and IG-017 bio-origin additives." Építőanyag - JSBCM 71.4, 2019. https://doi.org/10.14382/epitoanyag-jsbcm.2019.20

[3] Gömze, László A., Emese Kurovics, and Ludmila N. Gömze. “Changing the rheo-mechanical models of light metal Ti and Ti-alloy powders under uniaxial compaction.” Journal of Physics: Conference Series. Vol. 1045. No. 1. IOP Publishing, 2018. https://doi.org/10.1088/1742-6596/1045/1/012001

[4] Grigoriev, Mihail V., et al. “Deformation and fracture of alumina ceramics with hierarchical porosity.” Építőanyag - JSBCM 70.1, 2018. https://doi.org/10.14382/epitoanyag-jsbcm.2018.1

[5] Buyakov, A. S., et al. “Formation of pore structure in zirconia-alumina ceramics.” SCIENCE III. 109, 2018

[6] Gömze, László A., et al. “Development ceramic floor tiles with increased shear and pressure strengths.” Építőanyag – JSBCM, 70.1 2018. https://doi.org/10.14382/epitoanyag-jsbcm.2018.3

[7] Gömze, L. A., and L. N. Gömze. “Rheological principles of development hetero-modulus and hetero-viscous complex materials with extreme dynamic strength.” IOP Conference Series: Materials Science and Engineering. Vol. 175. No. 1. IOP Publishing, 2017. https://doi.org/10.1088/1757-899X/175/1/012001

[8] Gömze, A. L., and L. N. Gömze. “Rheo-mechanical model for self-healing asphalt pavement.” Journal of Physics: Conference Series. Vol. 790. No. 1. IOP Publishing, 2017. https://doi.org/10.1088/1742-6596/790/1/012001

[9] Kocserha, I., et al. “Characterisation of the wall-slip during extrusion of heavy-clay products.” Journal of Physics: Conference Series. Vol. 790. No. 1. IOP Publishing, 2017. https://doi.org/10.1088/1742-6596/790/1/012013

[10] Dedova, E. S., et al. “Structure and thermal behavior of zirconium tungstate under heating.” IOP Conference Series: Materials Science and Engineering. Vol. 140. No. 1. IOP Publishing, 2016. https://doi.org/10.1088/1757-899X/140/1/012007

[11] Kurovics, E., A. Y. Buzimov, and L. A. Gömze. “Influence of raw materials composition on firing shrinkage, porosity, heat conductivity and microstructure of ceramic tiles.” IOP Conference Series: Materials Science and Engineering. Vol. 123. No. 1. IOP Publishing, 2016. https://doi.org/10.1088/1757-899X/123/1/012058

[12] Kotova, O. B., A. V. Ponaryadov, and L. A. Gömze. “Hydrothermal synthesis of TiO2 nanotubes from concentrate of titanium ore of Pizhemskoe deposit (Russia).” Vestnik IG Komi SC UB RUS”1(253), (2016): 34-36. https://doi.org/10.19110/2221-1381-2016-1-34-36

[13] Gömze, L. A., et al. “Methods and equipment for the investigation of rheological properties of complex materials like convectional brick clays and ceramic reinforced composites.” Építőanyag -JSBCM (Online) 4 (2015): 143. http://dx.doi.org/10.14382/epitoanyag-jsbcm.2015.24

[14] Tihtih, M., et al. “Study on the effect of Bi dopant on the structural and optical properties of BaTiO3 nanoceramics synthesized via sol-gel method.” Journal of Physics: Conference Series. Vol. 1527. No. 1. IOP Publishing, 2020. https://doi.org/10.1088/1742-6596/1527/1/012043

[15] Inamuddin and M. Luqman, Ion exchange technology I: Theory and materials, Springer, New York, 2012.

[16] A. Dyer, An introduction to zeolite molecular sieves, John Wiley and Sons, Chichester, 1988.

[17] H. van Bekkum, E.M. Flanigen and J.C. Jansen, Introduction to zeolite science and practice, Studies in Surface Science and Catalysis 137, Elsevier Science B.V, Amestrdam, 2001.

[18] Kotova, Olga B., et al. “Composite materials based on zeolite-montmorillonite rocks and aluminosilicate wastes.” Építőanyag - JSBCM 71.4, 2019. https://doi.org/10.14382/epitoanyag-jsbcm.2019.22

[19] Buzimov, A. Y., et al. “Effect of Mechanical Treatment on the Structure and Properties of Natural Zeolite.” Inorganic Materials: Applied Research 9.5, 910-915. 2018. https://doi.org/10.1088/1742-6596/790/1/012004

[20] Buzimov, Alexandr Y., et al. “effect of mechanical treatment on properties of Si-Al-o zeolites.” Építőanyag (Online) 1: 23-26, (2018). https://doi.org/10.14382/epitoanyag-jsbcm.2018.1

[21] Buzimov, A. Y., et al. “Effect of mechanical treatment on properties of zeolites with chabazite structure.” Journal of Physics: Conference Series. Vol. 790. No. 1. IOP Publishing, 2017. https://doi.org/10.1088/1742-6596/790/1/012004

[22] Corma, A., et al. “Interaction of zeolite alumina with matrix silica in catalytic cracking catalysts.” Applied catalysis 66.1. 45-57, 1990. https://doi.org/10.1016/S0166-9834(00)81626-7

[23] Wongcharee, Surachai, Vasantha Aravinthan, and Laszlo Erdei. “Mesoporous activated carbon-zeolite composite prepared from waste macadamia nut shell and synthetic faujasite.” Chinese journal of chemical engineering 27.1, 226-236, 2019. https://doi.org/10.1016/j.cjche.2018.06.024

[24] Stocker, Kristina, et al. “Characterization and utilization of natural zeolites in technical applications.” BHM Berg-und Hüttenmännische Monatshefte 162.4, 142-147, 2017. https://doi.org/10.1007/s00501-017-0596-5

[25] Petranovskii, V., et al. “Potential uses of natural zeolites for the development of new materials: short review.” MATEC Web of Conferences. Vol. 85. EDP Sciences, 2016. https://doi.org/10.1051/matecconf/20168501014

[26] M. Barsoum, Fundamentals of Ceramics, Chap. 10, McGraw-Hill, New York, 1997.

[27] Johari, Izwan, et al. “Effect of the change of firing temperature on microstructure and physical properties of clay bricks from Beruas (Malaysia).” Science of Sintering 42.2 (2010): 245-254. https://doi.org/10.2298/SOS1002245J

Ref.:

Ibrahim, Jamal-Eldin F. M. – **Shushkov**, Dmitry A. – **Kurovics**, Emese – **Tihtih**, Mohammed – **Kotova**, Olga B. – **Pala**, Péter – **Gömze**, László A.: *Effect of composition and sintering temperature on thermal properties of Zeolite-Alumina Composite Materials*
Építőanyag – Journal of Silicate Based and Composite Materials, Vol. 72, No. 4 (2020), 131–134. p.
https://doi.org/10.14382/epitoanyag-jsbcm.2020.21

Mineral composition of bauxite residue and their surface for innovation materials

Olga B. KOTOVA ▪ Institute of Geology, FRC Komi SC, UB RAS, Russian Federation ▪ kotova@geo.komisc.ru
Ilia N. RAZMYSLOV ▪ Institute of Geology, FRC Komi SC, UB RAS, Russian Federation ▪ razmyslov-i@mail.ru
Jamal Eldin F. M. IBRAHIM ▪ Institute of Ceramics and Polymer Engineering, University of Miskolc, Hungary ▪ jamalfadoul@gmail.com
Dmitry A. SHUSHKOV ▪ Institute of Geology, FRC Komi SC, UB RAS, Russian Federation ▪ dashushkov@geo.komisc.ru

Érkezett: 2020. 06. 30. ▪ Received: 30. 06. 2020. ▪ https://doi.org/10.14382/epitoanyag-jsbcm.2020.22

Abstract
Natural aluminum ores and aluminosilicate residues are an important component in the development of strategies for the modification of composites, sorbents and other functional materials. The properties of bauxite and bauxite residue were studied by XRD, SEM and standard methods of mineral surface. The phase composition, magnetic, sorption and other properties of bauxite residue before and after exposure to chemical and physical methods to be used in industries are presented.

Keywords: bauxite residue, mineral composition, modification, advanced materials
Kulcsszavak: bauxitmaradvány, ásványi összetétel, módosítás, korszerű anyagok

Olga B. KOTOVA
is Head of Laboratory of Technology of Mineral Raw, Institute of Geology Komi SC UB Russian Academy of Sciences. Author and co-author of 10 books, 4 patents and more than 200 scientific articles. President of ICAM-2019. The member of Science Council of Russian Mineralogical Society.

Ilia N. RAZMYSLOV
is Junior Researcher, Laboratory of Comprehensive Assessment and Engineering of Georesources, Institute of Geology, FRC Komi SC, UB RAS. Author and co-author of 6 articles.

Jamal Eldin F. M. IBRAHIM
is a lecturer in the University of Bahri, Khartoum, Sudan, he graduated from University of Marmara, Istanbul, Turkey, Institute of Pure and Applied Sciences, Department of Metallurgical and Materials Engineering, for the time being, he is a PhD student in the University of Miskolc, Institute of Polymer and Ceramics Engineering, under supervision of Prof. L. A. Gömze.

Dmitry A. SHUSHKOV
is Researcher of Laboratory of Technology of Mineral Raw, Institute of Geology Komi SC UB Russian Academy of Sciences. Author and co-author of 2 patents and more than 40 scientific articles. Russian Mineralogical Society.

1. Introduction

Alumina is an important raw material for the development of the national economy; however, alumina production can result in great environmental problems. Potentially, bauxites are complex ores for aluminum, titanium, gold and rare elements, which determines the combined processing technologies to extract all useful components and use their technological properties [1-4]. Bauxite residue (red mud) are the main by-product of alumina production. Annually, up to 40 million tons of bauxite residue are resulted in the world, the bulk of which is still not used. The high alkalinity of such wastes adversely affects water, soil and air. Problems include the flow of alkaline solution and bauxite residue because of damaged pipelines or dams. High cost and large land area are also associated with the construction of dams. Bauxite residueis removed from the alumina plant outside the territory in the form of pulp and stored in a specially equipped site - the so-called mud lake. Dried bauxite sludge can be an effective filler of insulation materials, paints, mastics, tile and roll materials for flooring, etc. [1-8]. A significant part of the researches is devoted to composite materials based on aluminosilicates and technologies for modifying physicochemical properties to meet current and future requirements by request of companies involved in processing of raw materials and production of goods in factories. The study of aluminum and other metals is promoted by their attractiveness for many structural components, where special technological properties are important (increased strength, lower weight, etc.) [9-12]. Bauxite residue is a waste from alumina production, which is characterized by a high content of finely dispersed Fe, Al, and Ti oxyhydrides [8].

In recent years, protecting people and the environment from harmful effects of industrial pollution has become increasingly important. The use of sorbents wins a special recognition to solve a number of problems. The most widely used sorbents are natural clays characterized by chemical stability, mechanical strength, high ion-exchange selectivity for various compounds, low cost in comparison to synthetic organic ion exchangers and other inorganic materials [13-24]. For example, the papers [15-20] were devoted to composites based on analcime-montmorillonite rocks and aluminosilicate wastes (coal fly ash). An important role of integration of mineralogical and technological features of the material composition for predicting behavior in the technological processes of composite formation and their operational characteristics were emphasized.

Bauxite residue is also studied as sorbent [8, 13, 21]. The specific surface area of bauxite residue is 23–25 m^2/g, the density is 3.3–3.4 g/m^3, and the melting point is 1350–1370 °C. It was determined that the maximum sorption capacity of bauxite residue for strontium is 420 ± 24 mg-Eq/100 g. The high sorption properties of bauxite residue allow using it as a sorbent in the construction of technogenic barriers in places of radioactive waste burial.

The bauxite residuehasmineralogical characteristics (mineral and (or) phase composition), the form of occurrence of the useful component, morphostructural features that determine the strategy and tactics of their secondary use (*Fig. 1*):

- as raw without processing, for example, to recover valuable metals;
- as initial raw after additional processing to obtain industrial resources.

Even today we witness achievements in solving this problem, for example: storage, production of building materials, new materials to protect the environment, extraction of useful elements, etc. [1-22].

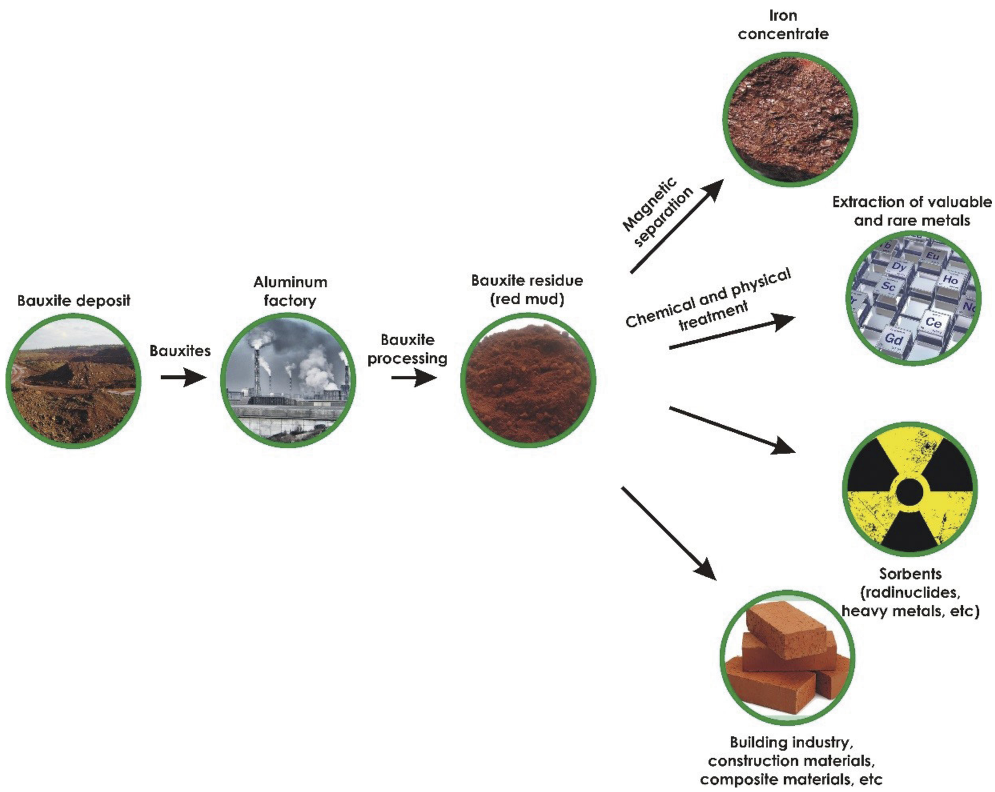

1. ábra A bauxit maradványok hasznosítása
Fig. 1 Utilization of bauxite residue

It is very important to study the surface of minerals of bauxite residue (in a fine state), taking into account their structural modification with the aim to process them efficiently. Sorption processes in the system (mineral-environment) were studied earlier. These processes (their mechanisms) are used, for example, to solve technological and environmental problems (for the extraction of non-ferrous metals from the effluents of metallurgical and other industries, the purification of liquid radioactive wastes, etc.) [10, 23], as well as in geochemical methods of searches for minerals, including migration and concentration (or dispersal) of various elements and formation of deposits [24].

Our task is to summarize the existing experience, including new data from our researches on bauxite residue, and to demonstrate the potential for practical implementation in various industries, to apply innovative methods for new materials.

2. Materials and experiments

2.1 Materials

Bauxite residue (red mud) – industrial wastes from the processing of bauxites from the Ural Aluminum Plant.

2.2 Methods of research

The chemical composition of the bauxite residue was determined by the silicate analysis. Phase diagnostics was carried out by X-ray diffraction (Shimadzu XRD-6000, CuK radiation). The microelement composition was determined by AES-ICP (ISP-22 Spectrograph). The specific surface area was determined by low temperature nitrogen adsorption method with the help of NOVA 1200e Quantachrome analyzer of surface area and pore size. The density was measured by the pycnometric method. The sorption of radionuclides was carried out according to the procedure described in [21]. Methods for studying the surface of minerals are described in [23, 24]. The surface study after laser processing was carried out by Raman spectroscopy (Raman scattering) using LabRAM HR800 high-resolution Raman spectrometer (Horiba, Jobin Yvon), and optical microscopy was performed with the help of Olympus BX41. The surface was modified by GOR-100M ruby laser with a wavelength λ = 694.3 nm and energy density of about 30 J/cm^2.

3. Results and discussion

3.1 Chemical and mineral composition

The chemical and mineral composition of bauxite residueis determined by the composition of the initial bauxite and processing methods. The composition varies, but not much. Thus, for example, Fe_2O_3 + FeO, CaO, Al_2O_3 (*Table 1*) are main components of the chemical composition of the bauxite wastes of the studied samples, the loss on ignition was 12.77%. X-ray analysis was used to diagnose hematite, calcite, lepidocrocite/goethite, nosean, pyrite, garnets, and X-ray amorphous iron compounds. The specific surface area was 18.7 m^2/g, density 2.84–2.94 g/cm^3. According to AES-ICP data, the bauxite residue contains significant amounts of REE exceeding bulk earth values. The microelement composition is shown in *Table 2*.

Component	Content, %	Component	Content, %
Fe_2O_3	34.18	CO_2	6.00
FeO	5.40	Na_2O	2.68
CaO	15.27	SO_3	2.53
Al_2O_3	12.17	H_2O^-	1.96
SiO_2	7.87	Sgen	1.66
TiO_2	3.27	P_2O_5	0.81
MgO	1.40	LOI	12.77

1. táblázat A bauxit maradvány kémiai összetétele
Table 1 Chemical composition of bauxite residue

Element	Sr	La	Zr	V	Ni	Ce	Y	Cu	Zn	Nd
Content, g/t	1716	602	602	421	282	282	233	192	167	158
Element	Pb	Ba	Li	Co	Sc	Nb	Ta	Be	Cd	-
Content, g/t	145	121	104	90	86	27	10	5	2	-

2. táblázat A bauxit maradvány mikroelemeinek összetétele
Table 2 Microelement composition of bauxite residue

3.2 Granulometric analysis

The bauxite residue is represented by a fine component, which complicates the extraction of useful minerals by traditional methods, such as magnetic separation. Gravity separation is preferable because it allows improving the content of berthierine in the tails and intermediate product of the concentration table 49-52%, against 43% related to magnetic separation. This is explained by significant differences in the densities of berthierine and hematite (3.0 - 3.4 g/cm^3 against 4.9 - 5.4 g/cm^3 respectively). Hematite is concentrated in fine fractions of bauxite residue, bertierine in larger fractions.

3.3 Bauxite residue as source of alumina, caustic alkali, iron and rare earths

From the alumina workshop of the plants, sludge as pulp enters the sludge storages, which pollute the environment and increase the cost of the main products of the plants. With dump bauxite residue, 10–20% of the alumina, contained in the initial bauxite, and 60–200 kg of Na_2O per 1 ton of marketable alumina are irretrievably lost. The annual loss of iron with bauxite residue from a large plant is about 0.5 million tons. Therefore, the bauxite residue should be considered as one of the potential sources of alumina, caustic alkali, iron and rare earth elements.

3.4 The effect of the condition of surface of bauxite residue minerals on the distribution of magnetic separation enrichment products

The finely dispersed state of bauxite residue unequivocally indicates a significant influence of the surface condition. Earlier, we studied the finely dispersed mineral–environment system [23, 24]. The value of the surface charge is important for sorption processes. The value and polarity of the surface charge depends on the position of the Fermi level. Thus, the Fermi level acts as a regulator of the activity of the surface of minerals [23] in sorption processes. When minerals are heated at temperatures 100-150 °C, the hydroxyl coating is broken, and we observe a shift of the point of zero charge of the mineral surface. As a result, we observe a change in the magnetic properties of the samples.

For example, under normal conditions, berthierine and hematite (bauxite residue minerals) possess close magnetic properties and are ineffectively separated by magnetic separation methods. Bertierine significantly reduces the quality of the iron concentrate because of a low content of the latter. For comparison, we carried out magnetic separation of the initial sludge and calcined one for 2 hours at 150 °C. After separation and calcination, the chemical composition of the samples was slightly different from each other (*Table 3*). Changes occurred in the yield and mineral composition of the calcined samples. The non-magnetic fraction of the calcined sample increased by 22% compared to the non-calcined sample. The diffraction patterns of the non-calcined samples (non-magnetic and magnetic fractions) are slightly different from each other. The calcined samples showed a changed mineral composition. Two main minerals are diagnosed in the composition of bauxite residue: berthierine (often confused with chamosite, the difference is the absence of 14 Å reflex in berthierine diffraction pattern) and hematite. The intensity of the main peak of berthierine at (7.03 Å) in the calcined non-magnetic sample is much lower than in the non-calcined and, conversely, in the calcined sample, the intensity of the peak of berthierine increases significantly. This gives reason to conclude that even a slight heat treatment (150 °C) (violation of the hydroxyl coating of the mineral) results in a change in the ratio of the yield of minerals in the non-magnetic and non-magnetic fractions.

Components	Chemical composition, wt. %			
	No calcination		Calcination	
	Non-magn.	Magn.	Non-magn.	Magn.
Mass, %	49	51	71	29
Fe_2O_3gen	4.12	5.24	4.52	5.13
Al_2O_3	2.41	2.21	2.21	2.29
SiO_2	6.50	6.74	7.02	7.71
SO_3	81.48	77.97	80.89	72.56
TiO_2	0.66	1.09	0.71	1.96
CaO	1.22	2.24	1.33	3.99
MnO	0.44	0.73	0.34	1.39
P_2O_5	3.11	3.72	2.92	4.86
SrO	0.06	0.08	0.06	0.12
Total	100.00	100.0	100.00	100.00

3. táblázat A vizsgált bauxitmaradványok tömegének és kémiai összetételének megoszlása
Table 3 Distribution of mass and chemical composition of studied bauxite residue

3.5 Sorption properties of bauxite residue

Bauxite residue is characterized by a high sorption activity against natural long-lived radionuclides – uranium, radium, thorium (U^{238}, Ra^{226}, Th^{223}). The kinetics of sorption of radionuclides by bauxite residue [21] showed that more than 95 and 97% of uranium and radium, respectively, are extracted from the solution within 30 minutes of interaction. After 2 hours, more than 98.8% of radium (the content in the solution is below the detection limit) is sorbed by bauxite residue. The distribution coefficient for radiation was more than 4040 ml/g. With increasing reaction time, uranium recovery increases slightly and reaches a value of 96.63%. Thorium sorption proceeds lower: after 1 h, about 20% is recovered, after 24 h – more than 60%. The study of desorption characteristics showed that sorbents had a high absorption strength (or low total desorption). When interacting with water and ammonium acetate, the desorption of radionuclides was less than 1%; during acid treatment, radium and uranium were most strongly retained (desorption was 6.3 and 11.6%, respectively), and radium was the least stable (up to 48.4% was desorbed into solution). The use of bauxite wastes as sorbents or additional material in various fields of technology does not solve the problem of processing large quantities of this waste product from alumina production. Therefore, in recent years, in many countries of the world, extensive research has been conducted on the recovery of valuable components from bauxite residue. A number of papers suggest to usebauxite residueas raw material for iron, gold, platinum, REE [2, 4, 8, 21, 25].

We studied the content of radioactive elements in bauxite and bauxite residue. For example, the thorium content in bauxite residue is about the same as in bauxite, uranium is 14 times lower, and radium is 10–6 times lower.

3.6 Modification of structure and properties

Bauxite residue is used as raw material for Fe production. For the effective development of this industrial product, technological enrichment schemes should provide for a low-waste process: along with obtaining iron-containing commodity concentrates, it is necessary to obtain concentrates of other available minerals, for example, valuable metals.

Bauxite residue, accumulated in tailings, undergo significant transformations during energy impacts in terms of micro- and nanodispersed oxyhydroxides of iron and REE, which optimizes a number of physical and technical properties of sludgeand expands the potential for practical implementation in various industries, while creating new materials. For example, in [4, 8], mechanisms of the conversion of weakly magnetic iron-containing minerals (hematite, goethite) to highly magnetic minerals (magnetite, maghemite) under the influence of external physicochemical factors were considered.

The laser agglomeration technology proposed in [25] is an alternative to cyanidation and amalgamation technologies, which has a negative impact on the environment.

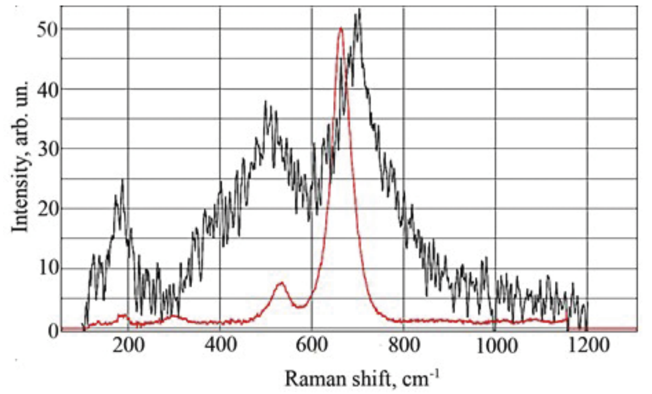

Fig2-1

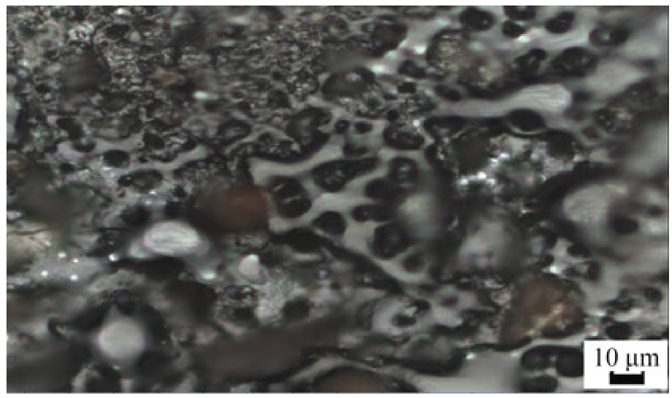

Fig2-2

2. ábra A Raman spektrum és a felület a besugárzási zónában
Fig. 2. Raman spectrum and surface in the irradiation zone

We determined that in the area of laser irradiation, the intensive formation of a new phase is taking place. According to Raman spectroscopy data, the newly formed phase is magnetite (*Fig. 2*). In this case, it is worth noting the heterogeneity of the magnetite film at the submicron level. The irradiation surface is a magnetite matrix interspersed with silica, hematite, pyrite.

The impact of laser irradiation on finemineral raw materials (bauxite residue) containing hard-to-enrich, colloidal gold and other noble metals, REE and RME results in agglomeration processes with the formation of coarse particles in the form of a drop-like shape with particle sizes one to two orders of magnitude larger than the original ones. As a result of laser melting, the substance is redistributed with the concentration and agglomeration of valuable metals (gold, platinum, hafnium, tungsten, bismuth, etc., the list depends on the experimental conditions), which are "invisible" before processing [25].

4. Conclusions

This article is devoted to the prospects of using bauxite residue as a source of metals and advanced materials. An important role of integration of mineralogical and surface features of rad mud for innovative new material were emphasized.Complex forms of occurrence of useful components of bauxite residue and their technological properties were revealed. We emphasized the influence of the surface state of bauxite residue minerals on their physical and chemical properties. It was noted that various physical and chemical influences on bauxite residue canresult in a fundamental improvement of their useful properties. The use of bauxite residue as an additional material (in composites, cement, etc.) does not solve the problem of processing large quantities of this dump product of alumina production. Therefore, we suggest using bauxite residue as raw material for metals, REE, etc. The use of bauxite residue as sorbent (radionuclides, heavy metals, etc.) is one of the promising areas of waste utilization.

Acknowledgements

The authors are thankful to Geonauka Center for Collective Use, where we conducted our studies. The reported study was funded by RFBR and NSFC according to the research project RFBR № 20-55-53019 and NSFC № 4191101331, 41672039. The studies were supported by the program "Main directions of integrated assessment and efficient use of georesources of Timan-Northern Ural-Barents Sea Region" GR AAAA-A19-119031390057-5.

References

[1] Kotova, O., Vakhrushev, A. (2011): Timan bauxites: Mineralogical and technological features. *Vestnik of Institute of Geology of Komi SC of UB of RAS.* No. 3, pp. 12-16.

[2] Kotova, O., Gasaleeva, G., Vakhrushev, A. (2015): Minerals of Bauxites and Residues: Problems of Processing and Enrichment (Russia). *In: Proceedings of the 11th International Congress for Applied Mineralogy (ICAM)*. Pp. 241-251.

[3] Kotova, O. B., Shushkov, D. A., Gömze A. L., Kurovics E., Ignatiev, G. V., Sitnikov, P. A., Ryabkov, Y. I., Vaseneva, I. N. (2019): Composite materials based on zeolite-montmorillonite rocks and aluminosilicate wastes. *Építőanyag–JSBCM*, Vol. 71, No.4, pp.125–130. https://doi.org/10.14382/epitoanyag-jsbcm.2019.22

[4] Razmyslov, I. N., Kotova, O. B., Silaev, V. I. et. al. (2019): Microphase Heterogenization of High-Iron Bauxite as a Result of Thermal Radiation. *J Min Sci.* Vol. 55, pp. 811–823. https://doi.org/10.1134/S1062739119056185

[5] Bolden, J. et al. (2013): Utilization of recycled and waste materials in various construction applications. *American Journal of Environmental Science* Vol. 9(1), pp. 14-24.

[6] Rahman, T., Mohajerani, A., Giustozzi, F. (2020): Recycling of Waste Materials for Asphalt Concrete and Bitumen: A Review. *J. Materials.* Vol. 13, 1495. https://doi.org/10.3390/ma13071495

[7] Czarnecki, L., VAN Gemert, D. (2017): Innovation in construction materials engineering versus sustainable development. *Bulletin of the Polish Academy of Sciences Technical Sciences.* Vol. 65, No. 6. https://doi.org/10.1515/bpasts-2017-0083

[8] Kotova, O. B., Razmyslov, I. N. (2018): Problems of processing and enrichment of bauxite, waste disposal. *Exploration and protection of mineral resources.* No. 10, pp. 51–55.

[9] Kumaravel, S., Alagumurthi, N. (2020): Material removal characteristics of Al-SiO_2 composite in WEDM. Építőanyag–*JSBCM.* Vol. 72, No. 1, pp. 20–24. p. https://doi.org/10.14382/epitoanyag-jsbcm.2020.4

[10] Gherissi, A., Ali, M. (2020): Superficial hardening improvement of nano and micro composite Al TiC. Építőanyag-*JSCM.* Vol. 72, No. 1, pp. 25–29. https://doi.org/10.14382/epitoanyag-jsbcm.2020.5

[11] Kurovics, E., Kotova, O. B., Gömze A. L., Shushkov, D. A., Ignatiev, G. V., Sitnikov, P. A., Ryabkov, Y. I., Vaseneva, I. N., Gömze, N. L. (2019): Preparation of particle-reinforced mullite composite ceramic materials using kaolin and IG-017 bio-origin additives. Építőanyag-*JSCM.* Vol. 71, No. 4, pp. 114–119. https://doi.org/10.14382/epitoanyag-jsbcm.2019.20

[12] Shmakova, A., Kanev, B., Gömze A. L., Kotova O. (2018): Crystal chemical characteristics and physical properties of ferrous minerals as the basis for the formation of functional materials. *Applied materials science II. Compilation of selected scientific papers.* pp. 17–21. (ISBN 978-615-00-3118-7)

[13] Amritphale, S., Anshul, A., Chandra, N., Ramakrishnan N. (2007): A novel process for making radiopaque materials using bauxite – Red mud. *Journal of the European Ceramic Society.* Vol. 27, Iss. 4, pp. 1945-1951, https://doi.org/10.1016/j.jeurceramsoc.2006.05.106

[14] Yang, S., Zhang, Y., Yu, J., Huang, T., Qi, T., Chu, P., Qi, L. (2014): Multi-functional honeycomb ceramic materials produced from bauxite residues. *Materials & Design*. Vol. 59, pp. 333–338. https://doi.org/10.1016/j.matdes.2014.02.061

[15] Kotova, O. B., Harja, M., Cretescu, I., Noli, F., Pelovski, Y., Shushkov, D. A. (2017): Zeolites in technologies of pollution prevention and remediation of aquation systems. *Vestnik of Institute of Geology of Komi SC UB RAS.* No. 5, pp. 49–53, http://doi.org/10.19110/2221-1381-2017-5-49-53

[16] Forminte (Litu), L., Ciobanu, G., Gómez De Castro, C., Kotova, O., Harja, M. (2018): Comparison between new complex coagulant from fly ash and Al/Fe coagulants. *4th International Conference on Chemical Engineering (ICCE 2018) - Innovative materials and processes for a sustainable development*. Iasi, Romania, 2018.

[17] Kotova, O., Harja, M., Broekmans, M.A.T.M., Gomez de Castro, C. (2018): New smart materials with application in medicine and environmental protection. *Proceedings of the 10th Edition of Euroinvent European exhibition of creativity and innovation*. Euroinvent 2018. 10-31 Mai 2018 "George Enescu", Iasi, Romania. P. 550.

[18] Harja, M., Ciobanu, G., Kotova, O. (2017): Comparative study regarding retention of zinc ions by different ion exchange resins. *Proceedings book: International Conference "New trends in environmental and materials engineering" (INVENT-INVEST 2017).* UNGHENI, ROMANIA-MOLDOVA, 12-15, Noiembrie, 2017. (published in the journal The Annals of "Dunarea de Jos" University of Galati, accredited CNCSIS and indexed in CSA)

[19] Harja, M., Kotova, O., Ciobanu, G., Litu, L. (2017): New adsorbent materials on the base of ash and lime for lead removal. *Proceedings book: International Symposium "THE ENVIRONMENT AND THE INDUSTRY".* SIMI 2017, Bucharest, Romania, September, 28-29, 2017. http://doi.org/10.21698/simi.2017.0009

[20] Kotova, O. B., Shushkov, D. A. – Gömze, A. L., Kurovics, E., Ignatiev, G. V., Sitnikov, P. A., Ryabkov, Y. I., Vaseneva, I. N. (2019): Composite materials based on zeolite-montmorillonite rocks and aluminosilicate wastes. Építőanyag-*JSBCM.* Vol. 71, No. 4, pp. 125–130. https://doi.org/10.14382/epitoanyag-jsbcm.2019.22

[21] Kotova, O. B., Moskalchuk, L. N., Shushkov, D. A., Leontyeva, T. G., Baklay, A. A. (2017): Radionuclide sorbents based on industrial wastes: physical-chemical properties and prospects for use. *Vestnik of Institute of Geology of Komi SC of UB of RAS.* No. 4, pp. 29–36. http://doi.org/10.19110/2221-1381-2017-4-29-36 (in Russian)

[22] Shushkov, D., Kotova, O., Shuktomova, I. (2013): Removal of radionuclides by analcime-bearing rocks. *J. Materials Science and Engineering.* Vol. 47, pp. 198–202, http://doi.org/10.1088/1757-899X/47/1/012041

[23] Kotova, O. (2013): Clay Minerals: Adsorbophysical Properties. *J. Materials Science and Engineering.* pp. 170-176.

[24] Ponaryadov, A., Kotova, O., (2020): Phosphate sorption on leucoxene. *Vestnik of Geosciences.* No 1, pp. 19—23. http://doi.org/10.19110/geov.2020.1.3

[25] Kotova, O., Leonenko, N. (2016): Physics and chemistry of minerals under laser processing. *IOP Conf. Ser.: Mater. Sci. Eng.* Vol. 123 012016. http://doi.org/10.1088/1757-899X/123/1/012016

Ref.:
Kotova, Olga B. – **Razmyslov**, Ilia N. – **Ibrahim**, Jamal Eldin F. M. – **Shushkov**, Dmitry A.: *Mineral composition of bauxite residue and their surface for innovation materials*
Építőanyag – Journal of Silicate Based and Composite Materials, Vol. 72, No. 4 (2020), 135–139. p.
https://doi.org/10.14382/epitoanyag-jsbcm.2020.22

Effect of bauxite grain size distribution on beneficiation and improvement of materials

Olga B. KOTOVA ▪ Institute of Geology, FRC Komi SC, UB RAS, Russian Federation ▪ kotova@geo.komisc.ru
Ilia N. RAZMYSLOV ▪ Institute of Geology, FRC Komi SC, UB RAS, Russian Federation ▪ razmyslov-i@mail.ru
Emese KUROVICS ▪ Institute of Ceramics and Polymer Engineering, University of Miskolc, Hungary ▪ fememese@uni-miskolc.hu
Aleksandr I. LVOVSKY ▪ MIREA, Russia ▪ alekslvo@yandex.ru
László A. GÖMZE ▪ Institute of Ceramics and Polymer Engineering, University of Miskolc, Hungary ▪ femgomze@uni-miskolc.hu

Érkezett: 2020. 06. 30. ▪ Received: 30. 06. 2020. ▪ https://doi.org/10.14382/epitoanyag-jsbcm.2020.23

Abstract
The rational use of the constituent aluminum-containing ores in the industry to create new functional materials is one of the promising trends of mineral processing and engineering. Chemical analysis was carried out by X-ray fluorescence method using Horiba MESA 500. Shimadsu XRD-6000 device was used for X-ray diffraction analysis. The particle size distribution was determined by LS 13 320 XR laser particle size analyzer (Beckman Coulter).
We compared results of X-ray phase and granulometric analyses. It was shown that the technology of deep fractionation of particles of high-iron bauxites and kaolinite clays improved the quality of raw materials and efficiency of use of minerals in enrichment processes and various industries, when creating functional materials.
Keywords: particle size distribution, high-iron bauxites, kaolinite clays, functional materials
Kulcsszavak: szemcseeloszlás, magas vastartalmú bauxitok, kaolinok, funkcionális anyagok

Olga B. KOTOVA
is Head of Laboratory of Technology of Mineral Raw, Institute of Geology Komi SC UB Russian Academy of Sciences. Author and co-author of 10 books, 4 patents and more than 200 scientific articles. President of ICAM-2019. The member of Science Council of Russian Mineralogical Society.

Ilia N. RAZMYSLOV
is Junior Researcher, Laboratory of Comprehensive Assessment and Engineering of Georesources, Institute of Geology, FRC Komi SC, UB RAS. Author and co-author of 6 articles.

Emese KUROVICS
is graduated from the University of Miskolc, Department of Ceramics and Silicate Engineering as a material engineer, where she continues her study as PhD student under supervision of Prof. L. A. Gömze

Aleksander I. LVOVSKY
is Engineer of the Department of Chemistry and Technology of Rare and Scattered Elements and Nanoscale composite materials named after K.A. Bolshakov of Russian Technological University (MIREA), Moscow, Russia. He is the author of 12 scientific articles, three copyright certificates and two patents.

Laszlo A. GOMZE
is establisher and professor of the Dept. of Ceramics and Silicate Engineering at Institute of Ceramics and Polymer Engineering, University of Miskolc

1. Introduction

Rising production and consumption of functional materials based on aluminum raw materials results in reducing mineral resources and formation of large volumes of wastes [1]. Environmental problems are becoming more pronounced. We need to find special ways to solve them. Information about the grain size distribution of bauxite plays a significant role in optimization of production systems in various branches of industry [2].

Middle Timan bauxites (Russia) – a valuable raw for aluminum production. Kaolinite clays and white bauxites are used to produce refractories. Middle Timan bauxites and kaolinite clays are genetically related; kaolinite clays, as a result of decomposition and removal of silica, were the basis for the formation of white bauxites. Their genetic affinity determines the similarity of their technological properties [4]. The main aluminum-containing mineral of the Middle Timan bauxites, boehmite, is also a component of kaolinite clays. For the successful development of aluminum-containing mineral raw and the development of technologies for its processing, it is necessary to know not only the chemical and mineral composition of the ores, but also their structural characteristics, including their granulometry.

The granulometric composition of the constituents of aluminum-containing ores is very important to determine the degree of grinding in technological processes. At present, grinding processes are the most energy-consuming, at the same time, under-grinding results in losses in processing of bauxite ore into alumina [5]. A significant part of the ore substance is concentrated in the finely dispersed and X-ray amorphous phases. This fraction of bauxite and clays can be used as a sorbent of heavy metals, nuclides and other pollutants, become a raw material for producing metals, and can be used in the building industry (for example, in the production of cement) [6-13].

In [5] the authors provide data on X-ray and synchrotron small-angle scattering. They note that finely dispersed particles of the order of 40 nm prevail in Middle Timan bauxites. The granulometric methods, tested earlier, have several drawbacks (the small-angle scattering method is limited to the range of 0.001-1 mcm and shows only effective particle sizes; the sieve analysis is limited for small particle sizes; the sedimentation method, based on the Stokes formula, does not take into account the real particle shape, for large particles it gives increased error, and for small particles requires a significant measurement duration), while the laser diffraction method is free from these drawbacks and gives a differential particle size distribution in a wide range of sizes (from tens nanometers to a few millimeters) with a high accuracy.

This work is devoted to identifying granulometric composition of bauxites and kaolinite clays (Vezhayu-Vorykvinskoe deposit, Russia) by laser diffraction to increase efficiency of use of minerals use in industry and to improve materials.

2. Materials ant experiments

2.1 Materials

We used samples of high-iron (VV-3) and low-iron (MZB-1) varieties of bauxites and kaolinite clays (VVK) (Vezhayu-Vorykvinskoe deposit, Russia).

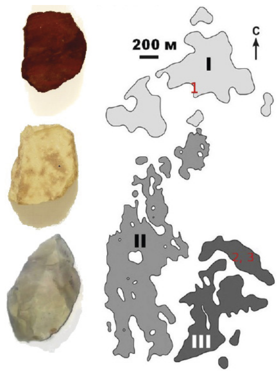

1. ábra Az alumíniumtartalmú nyers (balra) vizsgált típusai és a Vezhayu-Vorykvinskoe érclelőhelyeinek elhelyezkedése, Közép-Timán, Oroszország (jobbra). Felülről lefelé: hematit-boehmite bauxit, berthierine-boehmite alacsony vastartalmú bauxit, kaolinit agyag

Fig. 1 The studied types of aluminum-containing raw (left) and map of location of ore bodies of the Vezhayu-Vorykvinskoe deposit, Middle Timan, Russia (right). Top-down: hematite-boehmite bauxite, berthierine-boehmite low-iron bauxite, kaolinite clay

2.2 Methods of investigations

We measured the particles by laser analyzer LS 13 320 XR (Beckman-Coulter, USA). This instrument structurally combines the laser diffraction method with PIDS (Polarization Intensity Differential Scattering) to increase resolution and to ensure reliable measurement of submicron particles. The analyzer allows determining distribution of particles in the range from 10 nanometers to 3.5 millimeters.

The laser diffraction method uses the angular dependence of the intensity of the scattered light on the particle size. The indicated dependence is described by mathematical models of Fraunhofer and G. Mie. The Fraunhofer model is applicable for a particle size of at least 4-6 microns. This model is incorrect for smaller particles. To measure particles smaller than the specified size, it is necessary to use the G. Mie model, while the calculations take into account the refractive index of the particle material and the dispersion medium. For large particles, both models work equally correctly.

For reliable and reliable measurement of submicron particles, LS 13 320 XR analyzer uses PIDS technology based on the phenomenon of different intensities of scattering of vertically and horizontally polarized light. The specified technology provides a lower limit 10 nanometers.

Chemical analysis was carried out by X-ray fluorescence method using Horiba MESA 500; Shimadsu XRD-6000 instrument was used for X-ray diffraction analysis.

3. Results and discussion

3.1 Chemical composition

Table 1 shows that the bauxite samples are of high quality, with a high aluminum content, high silicon module (SM). VV-3 sample is a ferruginous variety of bauxite with SM 12.7. SM of MZB-1 sample–7.75. The bauxites are suitable for processing by the Bayer method. Kaolinite SM–VVK 0.85.

3.2 Mineralogical analysis

Phase analysis (*Fig. 2*) of the initial samples shows that ferriferous brown bauxite contains boehmite (predominant), hematite, goethite, gibbsite, rutile and possibly anatase. Low-iron bauxite contains boehmite, kaolinite, rutile, hematite as impurities. We determine kaolinite, boehmite, diaspore and rutile in kaolinite clay. *Table 2* shows approximate contents of basic minerals for each sample.

Samples	Content, %							
	Al_2O_3	Fe_2O_3	SiO_2	TiO_2	CaO	MgO	LOI	Sum
VV3	61.02	18.22	4.80	2.46	2.24	0.30	10.97	100.00
MZB-1	73.36	1.56	9.46	2.94	0.10	0.16	12.41	100.00
VVK	38.74	1.21	45.62	1.52	0.26	0.28	12.37	100.00

1. táblázat A vizsgált minták kémiai összetétele
Table 1 Chemical composition of the studied samples

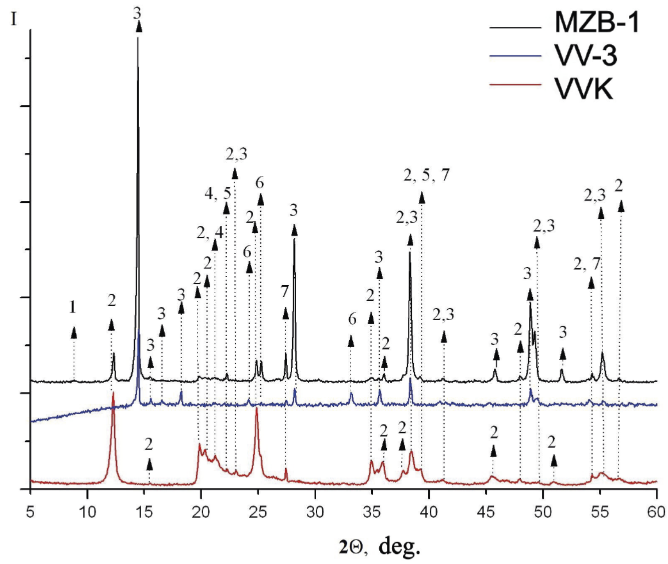

2. ábra A vizsgált minták röntgendiffraktogramjai. A számok a következő ásványoknak megfelelő csúcspozíciókat jelzik: 1 - földpát, 2 - kaolinit, 3 - boehmit, 4 - goetit, 5 - diaszpóra, 6 - hematit, 7 - rutil

Fig. 2 X-ray patterns of the studied samples. Numbers indicate peak positions corresponding to the following minerals: 1 - feldspar, 2 - kaolinite, 3 - boehmite, 4 - goethite, 5 - diaspore, 6 - hematite, 7 - rutile

Samples	Mineral phases, mass /volume fractions*, %				
	boehmite	hematite, goethite	Gibbsite	kaolinite, silica minerals	rutile, anatase
VV-3	39-40/47	36 (28+8)**/24	1-2/1.5	16/22	6/5
MZB-1	50-51/49	3-4/2	-	38/43	8/6
VVK	16-17/14	1-2/1	-	78-80/83	2/1.2

2. táblázat A vizsgált minták ásványi összetétele
Table 2 Mineral composition of the studied samples

* Volume fraction was calculated by weight contents and by densities ρ (g/l): boehmite - 3.02; hematite - 5.26; gibbsite - 2.3; kaolinite - 2.6; rutile - 4.2

** Hematite and goethite contents are shown in parentheses, respectively, based on the comparison of Mössbauer spectroscopy data

3.3 Granulometric analysis

A significant part of bauxite substance is represented by a fine component, which complicates bauxite processing by such traditional methods as magnetic separation. In [12, 13] the authors show that during crushing and grinding up to 90% of hematite of boehmite bauxite goes to 45 mcm class, and about 70% — to–20 mcm. The granulometric distribution and chemical composition for various size fractions of hematite-boehmite bauxite (VV-3 sample) are shown in *Fig. 3*.

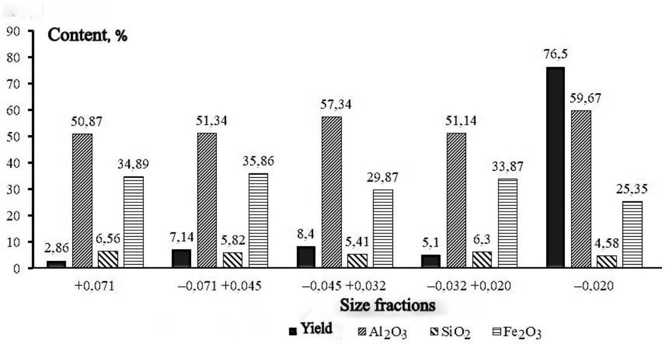

3. ábra A VV-3 minta. Az alapvető bauxit-oxidok megoszlása méret szerint
Fig. 3 VV-3 sample. Distribution of basic bauxite oxides by size

From the data on the material composition of these fractions it follows that the information is important both for preliminary processing of bauxite ore and selection of beneficiation technologies [6, 17], and when creating functional materials in various industries (X-ray radiation-shielding materials, ceramics, etc.) [18-20].

The authors [5] note that in Middle Timan bauxites, boehmite grains are concentrated in -5 µm class, a significant part of hematite and goethite are also concentrated in thin class (–0.5 µm), a gradual increase in the content of silicon dioxide is observed as reduction of grains from 10 mcm to 1 mcm and its sharp increase in the class –1 mcm, the latter is associated with the predominance of kaolinite, chamosite (berthierine).

A similar dependence was noted in [21], where, according to the distribution of the main kaolin oxides from the Zhuravlinny Log deposit, the content of iron and aluminum oxides increased for small classes. The Al_2O_3 content increases with decreasing size class: in the class 20-63 microns – 22.7%; in the class 10-2 microns – up to 33.2%; in the class 5-10 microns 36.2%; in -5 mcm – 36.93%. For the content of iron oxides, a multiple increase is observed in the fraction -5 microns, from 0.61% for the class 63-20 microns, to 1.27% for the class -5 microns. At the same time, a significant part of the kaolinite substance is in the fine fraction -63 microns – about 55.2% of the substance, and for -5 mcm – 35.6%.

Thus, the analysis of the composition of bauxite and kaolins by class showed the dependence of the content of certain minerals on particle sizes.

Using a laser particle analyzer, we established the size distribution of particles for a highly dispersed (clay) fraction, which accounts for 20-30% of the ore substance. The obtained data on the particle size distribution are presented in the form of graphs in *Fig. 4*.

The graphs have local extremes corresponding to several fractions. A general range from 0.3 to 20 mcm is observed for all samples.

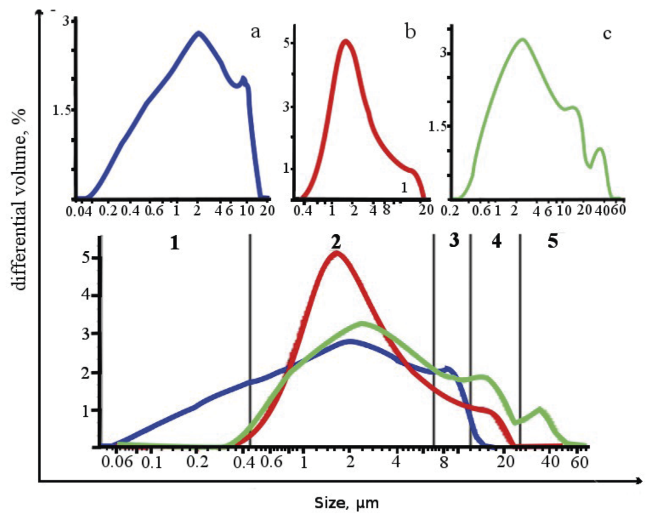

4. ábra A Vezhayu-Vorykvinskoe lelőhely nyílt gödöréből származó minták szemcseméretének megoszlása (kék - VV-3, piros - MZB-1, zöld - VVK). A számok a mély frakcionálás feltételes zónáit jelzik: 1 - hematit-goetit, 2 - boehmit, 3-5 szilikát (szilícium-dioxid, alumínium-szilikátok, berthierine), 4 - titán (rutil, anatáz)
Fig. 4 Differential particle size distribution for samples from open pits of the Vezhayu-Vorykvinskoe deposit (blue - VV-3, red - MZB-1, green - VVK). The numbers indicate conditional zones of deep fractionation: 1 - hematite-goethite, 2 - boehmite, 3-5 silicate (silica, aluminosilicates, berthierine), 4 - titanium (rutile, anatase)

The particle size distribution for each sample has its own specifics (see *Fig. 3*). Comparison of the data of X-ray phase and particle size analyses, as well as literature, showed that the number of mineral phases correlated with the number of local extremes. In *Fig. 4* several zones, corresponding to the mineral phases (hematite-goethite, boehmite silicate, titanium, silicate kaolinite), can be distinguished.

There is a correlation in the distribution of volume fractions of the substance of bauxite and kaolinite clays in the ranges of these fractions (*Table 3*). The results conform with published data on the distribution of boehmite, hematite, goethite, and silica-containing minerals in the clay fraction [5].

Innovative processing methods are being developed for fine bauxite and kaolinite clay substances. For example, in [22-24] the authors show that radiation-thermal treatment in the studied

Size fractions, mcm	0,01-0,5	0,5-6	6-10	10-25	25-60
Ranges	1	2	3	4	5
Mineral phases	hematite- goethite	boehmite	silicate	titanium	silicate-kaolinite
Samples			Volume, %		
VV-3	24.42	61.66	1.47	2.49	-
MZB	1.7	83.29	8.25	6.76	-
VVK	2.5	66.77	11.87	14.17	4.7

3. táblázat A bauxit és a kaolinit agyagok térfogatfrakcióinak megoszlása
Table 3 Distribution of volume fractions of substance of bauxite and kaolinite clays in the ranges of these fractions

iron bauxites results in a significant phase heterogenization, which opens the possibility of efficient extraction of industrial components from non-standard bauxites and red muds by environment-friendly methods.

4. Conclusions

The article compares data of X-ray phase and particle size analyses. Based on them, we have revealed a correlation between mineral phases of samples of Al ores of the Vezhayu-Vorykvinskoe deposit and corresponding extrema on the differential particle size distribution curves. The particle size distribution curves depend on the degree of resistance of mineral aggregates to mechanical stress, which is conditioned by the composition of these aggregates. Such technologies are promising for express assessment of quality of the ores at bauxite deposits.

New methods and approaches to technologies of deep fractionation of high-iron bauxite and kaolinite clays using LS 13 320 XR particle analyzer (based on the laser diffraction method and PIDS technology) allow determining particle size distribution and correlate ranges of size fractions with volume fractions of the specified minerals (boehmite, hematite, goethite and silica-containing minerals) and, thus, contribute to improve the quality of raw materials and the efficiency of mineral use in industry, when creating functional materials.

Acknowledgments

The authors are thankful to Beckman Coulter LLC and Geonauka Center for Collective Use, where we conducted our studies. The reported study was funded by RFBR and NSFC according to the research project RFBR № 20-55-53019 and NSFC № 4191101331, 41672039. The studies were supported by the program “Main directions of integrated assessment and efficient use of georesources of Timan-Northern Ural-Barents Sea Region” GR AAAA-A19-119031390057-5.

References

[1] Ozhogina, E. Kotova, O. (2019): New methods of mineral processing and technology for the progress of sustainability in complex ore treatment. Canadian Institute of Mining, Metallurgy and Petroleum, pp. 32-40, 2-s2.0-85059377649

[2] Litu L. Ciobanu G. Cimpreanu S. Kotova O. Cioccinta R. Bucur D. Harja M. (2019): Comparative study between flocculation-coagulation process in raw/wastewater treatment AgroLife Sci. J. Vol. 8, No.1, pp.139–145.

[3] Harja M. Kotova O. Sun S. Ponaryadov A. Shchemelinina T. (2019): Efficiency evaluation for titanium dioxide-based advanced materials in water treatment. In: Glagolev S. (Ed.): ICAM 2019, SPEES, pp. 255–258. https://doi.org/10.1007/978-3-030-22974-0_61

[4] Silaev V.I., Khazov A.F., Piskunova N.N. (2011): Assessment of mineral deposits: chemistry, geochemistry or mineralogy. In: Mineralogical and technological evaluation of mineral deposits and the problems of mineral discovery. Collection of articles on the materials of the V Russian seminar on technological mineralogy. Petrozavodsk - Karelian SC RAS, pp. 35-46.

[5] Kotova O. B., Vakhrushev A. V. (2011): Timan bauxites: Mineralogical and technological features. Vestnik of the Institute of Geology of the Komi Scientific Center, Ural Branch of the Russian Academy of Sciences. No. 3, pp. 12-16.

[6] Beavogi M., Balmaev B. (2017): Influence of granulometric composition of bauxite on the degree of extraction at the Fria alumina refinery (Republic of Guinea). GIAB, No. 9, pp. 131-138.

[7] Kotova O. (2019): New adsorbent materials on the base of minerals and industrial waste. IOP Conf. Series: Materials Science and Engineering 613, 012042.

[8] Kotova, O. B., Shushkov, D. A., Gömze A. L., Kurovics E., Ignatiev, G. V., Sitnikov, P. A., Ryabkov, Y. I., Vaseneva, I. N. (2019): Composite materials based on zeolite-montmorillonite rocks and aluminosilicate wastes. Építőanyag–JSBCM, Vol. 71, No.4, pp.125–130. https://doi.org/10.14382/epitoanyag-jsbcm.2019.22

[9] Kormshchikova Z.I. (2011): Comparative analysis of high-modulus bauxite as a raw material for structural material. In: Mineralogical and technological evaluation of mineral deposits and the problems of mineral disclosure. Petrozavodsk: Karelian Scientific Center of the Russian Academy of Sciences, pp. 158- 163.

[10] Kotova O., Gasaleeva G., Vakhrushev A. (2015): Minerals of Bauxites and Residues: Problems of Processing and Enrichment (Russia). In: Proceedings of the 11th International Congress for Applied Mineralogy (ICAM), pp 241-251.

[11] Shchemelinina T., Gömze L., Kotova O., Ibrahim J.E.F.M., Shushkov D., Harja M., Ignatiev G., Anchugova E. (2019): Clay- and zeolite-based biogeosorbents: modeling and properties, Építőanyag – JSBCM, Vol. 71, No. 4, pp. 120–124, https://doi.org/10.14382/epitoanyag-jsbcm.2019.21

[12] Kurovics, E., Kotova, O. B., Gömze A. L., Shushkov, D. A., Ignatiev, G. V., Sitnikov, P. A., Ryabkov, Y. I., Vaseneva, I. N., Gömze, N. L. (2019): Preparation of particle-reinforced mullite composite ceramic materials using kaolin and IG-017 bio-origin additives. Építőanyag-JSCM. Vol. 71, No. 4, pp. 114–119. https://doi.org/10.14382/epitoanyag-jsbcm.2019.20

[13] Ibrahim Jamal Eldin F. M., Gömze L. Kotova O. Shchemelinina T. Shushkov D. Ignatiev G. Anchugova E. (2019): The influence of composite, microstructure and firing temperature on the density, porosity, and shrinkage of new zeolite-alumina composite material, Építőanyag–JSBCM, Vol. 71, No. 4, pp. 120–124, https://doi.org/10.14382/epitoanyag-jsbcm.2019.21

[14] Vakhrushev A.V., Ulyashev V.V., Petrakov A.P. (2011): Study of the structure of low-iron bauxite by the method of synchrotron small-angle scattering. Materials of the 20th scientific conference of the Institute of Geology of the Komi Scientific Center, Ural Branch of the Russian Academy of Sciences “Structure, substance, history of lithosphere of the Timan-Northern Ural segment”. Syktyvkar: Geoprint (in Russia)

[15] Razmyslov I.N. (2016): Phase changes of bauxite minerals under energy influences. Vestnik of the Institute of Geology, Komi Scientific Center, Ural Branch of the Russian Academy of Sciences, No. 6 (258), pp. 33-34, https://doi.org/10.19110 / 2221-1381-2016-6-33-34

[16] Kotova, O. Razmyslov, I. Rostovtsev, V. Silaev, V. (2016): Thermal Radiation-Induced Modification of High-Iron Bauxites during Their Processing, Obogashch. Rud,, No. 4, pp. 16–22.

[17] Petrakis, E., Bartzas G., Komnitsas K. (2020): Grinding Behavior and Potential Beneficiation Options of Bauxite Ores, Minerals, Vol. 10 No.4, p. 314, https://doi.org/10.3390/min10040314

[18] Kong, L., Bao, J., Chen, L., Fan, Z., Li, W., Nikolic, H., Liu, K. (2018): Bauxite-modified oxygen carrier for chemical looping combustion: A possible solution to the heat of combustion compensation, Chemical Engineering Research and Design, V. 131, pp 635-642 https://doi.org/10.1016/j.cherd.2017.12.016

[19] Amritphale, S., Anshul, A., Chandra, N., Ramakrishnan N. (2007): A novel process for making radiopaque materials using bauxite—Red mud, Journal of the European Ceramic Society, V. 27, Issue 4, pp. 1945-1951, https://doi.org/10.1016/j.jeurceramsoc.2006.05.106

[20] Yang, S., Zhang, Y., Yu, J., Huang, T., Qi, T., Chu, P., Qi, L. (2014): Multi-functional honeycomb ceramic materials produced from bauxite residues, Materials & Design. V 59, pp. 333-338, https://doi.org/10.1016/j.matdes.2014.02.061

[21] Shamrikov A.S. (2002): Technology of enrichment and stabilization of ceramic properties of kaolins of the Zhuravlinny Log deposit, Tomsk. P. 217. (in Russia)

[22] Kotova, O. Lezina, O. Nazarova, L. Rubtsova, S. Ryabkov, Y. (2012): New technological solutions for ore concentration and recovery of valued minerals, Vestnik of Institute of Geology of Komi SC of UB of RAS. No. 10, pp. 32-34.

[23] Razmyslov, I., Kotova, O., Silaev, V., Lazlo, G. (2019): Phenomenon of Microphase Heterogenization by Means of Endocrypt-Scattered Impurity of Rare and Noble Metals as a Result of Radiation by Accelerated Electrons of Bauxites, 14th International Congress for Applied Mineralogy (ICAM2019), pp. 133-135, https://doi.org/10.1007/978-3-030-22974-0_31

[24] Razmyslov, I.N., Kotova, O.B., Silaev, V.I. et al. (2019): Microphase Heterogenization of High-Iron Bauxite as a Result of Thermal Radiation. J Min Sci Vol. 55, pp. 811–823. https://doi.org/10.1134/S1062739119056185

Ref.:

Kotova, Olga B. – **Razmyslov**, Ilia N. – **Kurovics**, Emese – **Lvovsky**, Aleksandr I. – **Gömze**, László A.: *Effect of Bauxite Grain Size Distribution on Beneficiation and Improvement of Materials*
Építőanyag – Journal of Silicate Based and Composite Materials, Vol. 72, No. 4 (2020), 140–143. p.
https://doi.org/10.14382/epitoanyag-jsbcm.2020.23

Characterization of phase transformation and thermal behavior of Sedlecky Kaolin

EMESE KUROVICS ▪ Institute of Ceramics and Polymer Engineering, University of Miskolc, Hungary ▪ fememese@uni-miskolc.hu
OLGA B. KOTOVA ▪ Institute of Geology, Komi Science Center, Ural Branch of the Russian Academy of Sciences, Russian Federation ▪ kotova@geo.komisc.ru
JAMAL ELDIN F. M. IBRAHIM ▪ Institute of Ceramics and Polymer Engineering, University of Miskolc, Hungary ▪ jamalfadoul@gmail.com
MOHAMMED TIHTIH ▪ Institute of Ceramics and Polymer Engineering, University of Miskolc, Hungary ▪ medtihtih@gmail.com
SHIYONG SUN ▪ Key Laboratory of Solid Waste Treatment and Resource Recycle of Ministry of Education, School of Environment and Resource, Southwest University of Science and Technology, China ▪ shysun@swust.edu.cn
PÉTER PALA ▪ Refratechnik Hungaria Ltd, Hungary
LÁSZLÓ A. GÖMZE ▪ Institute of Ceramics and Polymer Engineering, University of Miskolc, Hungary, IGREX Engineering Service Ltd. ▪ femgomze@uni-miskolc.hu
Érkezett: 2020. 06. 30. ▪ Received: 30. 06. 2020. ▪ https://doi.org/10.14382/epitoanyag-jsbcm.2020.24

Abstract
The authors have examined how the properties are changing using different sintering temperature based on the kaolin. Kaolin powder and a mixture of kaolin and 10 m% alumina was made and measured their sintering properties (TG, DTG, DTA, height). Pellets were compacted from the powders and sintered at 450 °C, 575 °C, 775 °C, 870 °C, 1100 °C temperature. The volume shrinkage, sintering weight losses, microstructure and phase composition of sintered specimens were investigated. In the case of sintering at 450 °C the volume of the samples increased; with a further increase of the temperature a continuous volume decrease can be observed.
Keywords: alumina, derivatograph, kaolin, mullite, XRD
Kulcsszavak: alumínium-oxid, derivatográf, kaolin, mullit, XRD

Emese KUROVICS
is graduated from the University of Miskolc, Department of Ceramics and Silicate Engineering as a material engineer, where she continues her study as PhD student under supervision of Prof. L. A. Gömze.

Olga B. KOTOVA
is professor and Head of Laboratory of Technology of Mineral Raw, Institute of Geology, Komi Science Center, Ural Branch of the Russian Academy of Sciences. Author and co-author of 4 patents and more than 150 scientific articles. Vice-president of International Commission on Applied Mineralogy (IMA-ICAM). Member of Russian Mineralogical Society.

Jamal Eldin F. M. IBRAHIM
is a lecturer in the University of Bahri, Khartoum, Sudan, he graduated from University of Marmara, Istanbul, Turkey, Institute of Pure and Applied Sciences, Department of Metallurgical and Materials Engineering, for the time being, he is a PhD student in the University of Miskolc, Institute of Polymer and Ceramics Engineering, under supervision of Prof. L. A. Gömze.

Mohammed TIHTIH
Is a lecturer in the Sidi Mohamed Ben abdellah University, Morocco, he graduated from Faculty of sciences Dhar El Mahraz, Fez, Morocco, Department of Physics, for the time being, he is a PhD student in the University of Miskolc, Institute of Ceramics and Polymer Engineering, under supervision of Prof. L. A. Gömze

Péter PALA
Is a chemical engineer who finished his study at the University of Pannonia. He has been working in the ceramics industry since 2003, at present he is the managing director of Refratechnik Hungaria Ltd.

László A. GÖMZE
is establisher and professor of the Department of Ceramics and Silicate Engineering in the University of Miskolc, Hungary. He is author or co-author of 2 patents, 6 books and more than 300 scientific papers.

1. Introduction

In the case of ceramics, the used drying and sintering methods greatly influences the properties of the product [1-7], so it is important to know the effect of sintering temperature. Because of this both in the traditional and in the technical ceramic industry there are a significant role of selected temperature and the condition (atmosphere) of the heat treatment [8-13]. The heat treatment affects the composition, physical, mechanical and functional properties of the product [10-18]. The phase diagrams can help to plan the composition of the final product from the raw materials. Even the simple materials systems like Al_2O_3 - SiO_2 also has been studied by many researchers. Two phase diagrams of Al_2O_3 - SiO_2 system are shown in *Fig. 1* [19-20]. The alumina-hydro-silicates such as the conventional kaolinite can also study partly with these phase diagrams, because they can show their thermal decomposition [21-22]. Many studies can be read regarding to the thermal properties of kaolin [23-26] and its kinetic analysis [27-28]. Kaolin and other clay minerals are usually raw materials obtained from nature which are widely used in the ceramic industry [29-32]. These materials may contain several contaminants and oxides, which may change the phases formed during heat treatment and their amount compared to what is theoretically expected.

In this research the authors have examined how the Sedlecky ml kaolin and alumina powder mixture behave under heating using a derivatograph and a heating microscope [33]. From the powder mixture ceramic specimens were also made to determine how the volume, weight and phases are changing using different sintering temperatures.

2. Materials and experiments

For the tests, kaolin and a mixture of kaolin and 10 m% alumina was milled in Retsch PM 400 planetary ball mill for 20 min at 150 rpm. The sintering behavior of powders were measured with a Camar Elettronica heating microscope and a MOM Derivatograph-C. During the tests, the furnaces were heated up to 1200 °C at a heating rate of 12 °C/min. The heating microscope took photos every 5 °C.

Specimens were made from the mixtures with uniaxially pressing method using a 100 kN mechanical pull-press machine. The pressed specimens were sintered in an electrical chamber kiln using different maximum kiln temperature and were kept at this temperature for 3 hours (*Fig. 2*).

The maximum temperature for sintering was chosen based on the SiO_2-Al_2O_3 phase diagram [20], waiting for the following phase transitions: 450 °C – kaolinite–metakaolinite;

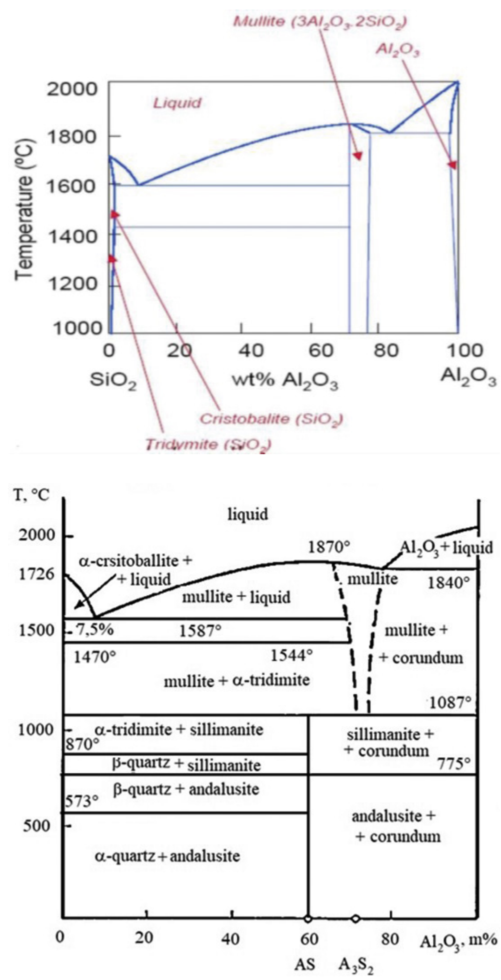

1. ábra SiO_2-Al_2O_3 rendszer normál körülmények között (átvéve L. Gömze A., 2001 [16] N M Bobkova 2007 [17])
Fig. 1 SiO_2-Al_2O_3 system at normal (Taken from L. A. Gömze, 2001 [19] N M Bobkova 2007 [20])

2. ábra A 450 °C, 575 °C, 775 °C, 870 °C és 1100 °C hőmérsékleten szinterelt minták
Fig. 2 The specimens sintered at 450 °C, 575 °C, 775 °C, 870 °C, 1100 °C temperature

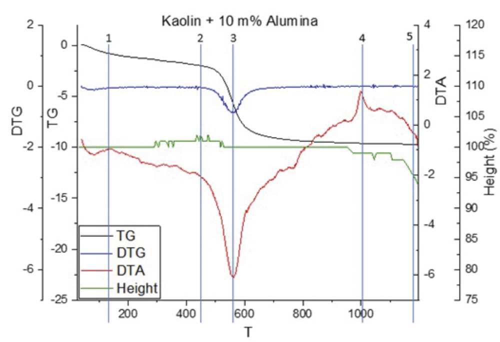

3. ábra Kaolin és alumínium-oxid keverék termoanalitikai görbéi
Fig. 3 Thermo-analytical curves of kaolin and alumina mixture

575 °C – α-quartz–β-quartz; 775 °C – andalusite–sillimanite; 870 °C – β-quartz–tridymite; 1100 °C – metakaolinite–mullite transitions. As the sintering temperature increases, the color of the specimens changes continuously. When the sintering temperature achieved 1100 °C the specimens became white. The change in color may indicate that the expected phase transitions have occurred. The properties of sintered specimens were measured, like volume shrinkage, sintering weight losses, microstructure, phase composition. The microstructures were examined by Hitachi TM-1000 scanning electron microscopy and XRD pattern were recorded with a Rigaku MiniFlex II X-ray diffractometer.

3. Results and discussions

The results of the thermo-analytical test of the kaolin-alumina mixture are shown in *Fig. 3*. From the achieved curves can be distinguish between drying 1, thermal degradation of kaolin 2-3 (conversion to metakaolin), formation of mullite 4 and sintering point 5 (where by the Camar Electronic the height of the sample compared to the original is 95%).

Sintering at 450 °C increases the volume of specimens while decreasing their mass. At 575 °C, a weight loss of more than 10% is observed, which is because of the kaolinite-metakaolinite conversion is complete. The kaolinite mineral loses its crystalline water content (kaolinite mineral composition: 39.52 m% Al_2O_3, 46.52 m% SiO_2, 13.96 m% H_2O). The change in mass from 575 °C was already slightly influenced by the added Al_2O_3 content. The initial volume of specimens and the volume of specimens sintered at 1250 °C were approximately the same for both mixtures (*Fig. 4*).

Some fracture samples were taken from the sintered specimens to examine the microstructure changes depending on the used maximum temperature. The fracture surface of the KA samples can be seen in the *Fig. 5* where the characteristics structure of the clay minerals and the added fine-grained alumina are well observable.

The mineral composition was not significantly affected by the addition of Al_2O_3 and is present throughout the corundum phase in the samples due to the low sintering temperatures. The XRD pattern shown in the *Fig. 6*. The mineral composition of the samples from the used kaolin sintered at 450 °C contain α-quartz and clay minerals like kaolinite and muscovite. In the experiment as the sintering temperature increased, the phase transitions took place as expected. Thus, the XRD pattern of the samples prepared during the research confirm the Al_2O_3-SiO_2 phase diagram found in Bobkova's book [20]. During the sintering at 1100 °C, the mullite phase was formed (*Table 1*). The proportion of crystalline phase is higher due to the addition of Al_2O_3 in the KA mixture. The ratio of mullite to tridymite was the same for both mixtures (mullite/tridymite ~ 10.6).

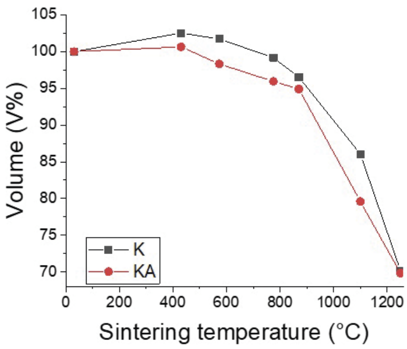

a)

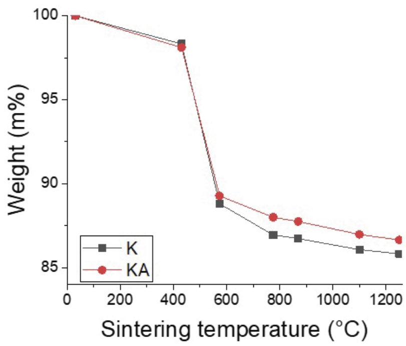

b)

4. ábra Az (a) térfogat és a (b) tömeg változása különböző hőmérsékleten
Fig. 4 The changing of volume (a) and weight (b) using different temperature

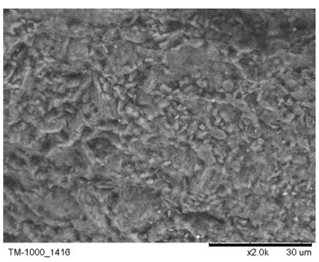

450 °C

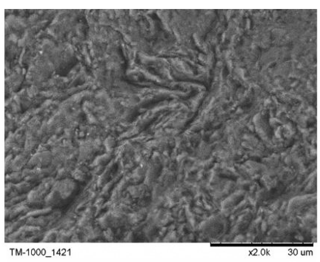

575 °C

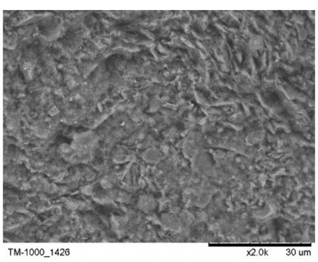

775 °C

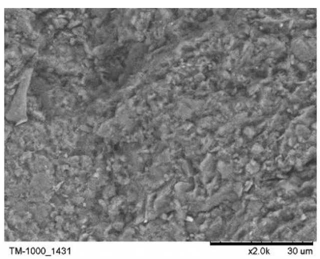

870 °C

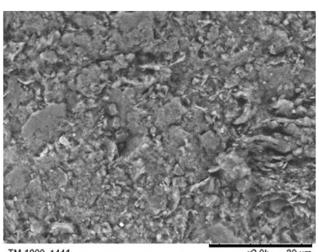

1100 °C

5. ábra A különböző hőmérsékleten szinterelt KA minták töretfelületének mikroszerkezete
Fig. 5 The microstructure of the fracture surface of the KA specimens sintered at different temperature

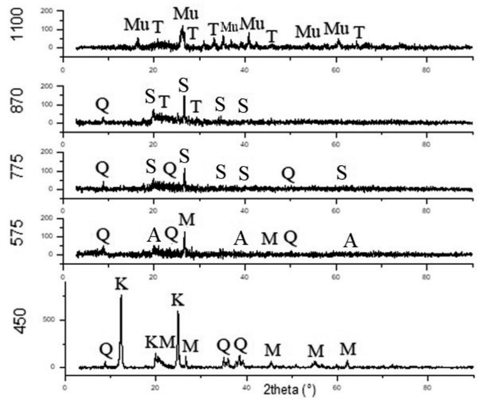

a)

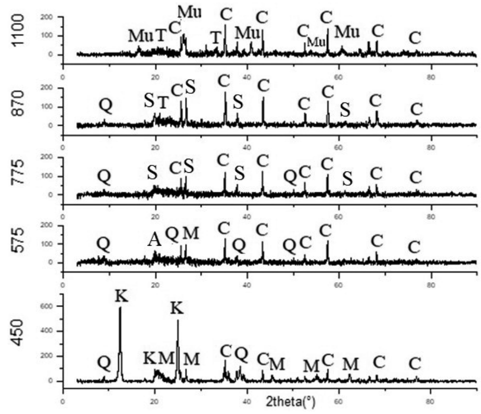

b)

6. ábra A K (a) és KA (b) minta XRD mintája különböző szinterezési hőmérsékleten (A-andalúzit, C-korund, K-kaolinit, M-muszkovit, Mu-mullit, S-szillimanit, T-tridimit, Q-kvarc)
Fig. 6 The XRD pattern for sample K (a) and KA (b) at different sintering temperature. (A-andalusite, C-corundum, K-kaolinite, M-muscovite, Mu-mullite, S-sillimanite, T-tridymite, Q-quartz)

Sign of the mixture		K	KA
Phase content, m%	Amorph	61.4	47
	Crystalline	38.6	53
	mullite	91.45	63.13
	tridymite	8.55	5.97
	corundum	-	30.9

1. táblázat 1100 °C-on szinterelt minták fázisaránya
Table 1 Phase ratio for samples sintered at 1100 °C

4. Conclusions

In this research work the Sedlecky ml kaolin as a traditional ceramic raw material were studied. The authors investigated how the microstructure, the phase composition changes depending on the used sintering temperature and how they will be changing when a small amount (10 m%) alumina were added to the kaolin raw mineral. From the experiments of derivatograph and heating microscopy investigation it can be concluded that both kaolin (K) and mixed (KA) powders shown the characteristic thermal curve of kaolin. The SEM and XRD results of the sintered specimens also confirm that 10 m% alumina has no significant effect on the sintering properties compering the pure kaolin when low sintering temperatures are used but it can be seen that at 1100 °C the proportion of crystalline fraction is significantly higher in the case of the alumina-containing mixture due to the corundum phase. The added alumina affects the functional properties of the ceramic products.

Acknowledgements

The described article was carried out as part of the EFOP-3.6.1-16-00011 "Younger and Renewing University – Innovative Knowledge City – institutional development of the University of Miskolc aiming at intelligent specialisation" project implemented in the framework of the Széchenyi 2020 program. The realization of this project is supported by the European Union, co-financed by the European Social Fund.

References

[1] L. A. Gömze, L. N. Gömze (2008): Relations between the material structures and drying properties of ceramic bricks and roof tiles, Építőanyag-JSBCM. Vol. 60. No.4. p.102 http://dx.doi.org/10.14382/epitoanyag-jsbcm.2008.16

[2] Kulkov S. N., Grigoriev. M. V. (2010): Sintering of Al_2O_3 ceramics based on different sizes powders. Építőanyag-JSBCM. Vol. 62. No.3. pp.66–69. http://dx.doi.org/10.14382/epitoanyag-jsbcm.2010.13

[3] Kurovics E., Buzimov A. Y., Gömze A. L. (2016): Influence of raw materials composition on firing shrinkage, porosity, heat conductivity and microstructure of ceramic tiles. IOP Conf. Ser.: Mater. Sci. Eng. Vol. 123. 012058 https://doi.org/10.1088/1757-899X/123/1/012058

[4] Ibrahim J. E. F. M., Gömze A. L., Kotova O. B., Shchemelinina T. N., Shushkov D. A., Ignatiev G. V., Anchugova E. M. (2019): The influence of composition, microstructure and firing temperature on the density, porosity, and shrinkage of new zeolite-alumina composite material. Építőanyag – JSBCM Vol. 71. No.4 pp. 120–124. https://doi.org/10.14382/epitoanyag-jsbcm.2019.21

[5] Kurovics E., Kulkov S. N., Gömze A. L. (2018): Investigation of ceramic brick rods with blackened materials inside. Építőanyag-JSBCM Vol. 70. No.1. p. 3 https://doi.org/10.14382/epitoanyag-jsbcm.2018.1

[6] J. F. M. Ibrahim, E. Kurovics, M. Tihtih, P. Somdee, A. G. Gerezgiher, K. Nuilek, E. E. Khine and M. Sassi (2020): Preparation and Investigation of Alumina-Zeolite Composite Materials. J. Phys.: Conf. Ser. Vol. 1527, 012029 https://doi.org/10.1088/1742-6596/1527/1/012029

[7] T. S. Aarnæs, M. Tangstad, (2019): Effect of H_2 on SiO and SiC formation, Építőanyag – JSBCM Vol. 71, No. 6, 194–197. p. https://doi.org/10.14382/epitoanyag-jsbcm.2019.34

[8] M. M. Abdelfattah, I. Kocserha, R. Géber (2019): The effect of calcium fluoride on mineral phases and properties of lightweight expanded clay aggregates. XIIIth Preparation of Ceramic Materials p. 141 ISBN: 978-80-553-3314-4

[9] E. Kurovics, B. Udvardi, K. Román, J. E. F. M. Ibrahim, L. A. Gömze (2019): Examination of the carbonization process using kaolin and sawdust. WIT Transactions on Engineering Sciences Vol. 124 p. 17 https://doi.org/10.2495/MC190021

[10] E. Kurovics, O. B. Kotova, L. A. Gömze, D A Shushkov, G. V. Ignatiev, P. A. Sitnikov, Y. I. Ryabkov, I. N. Vaseneva, L. N. Gömze (2019): Preparation of particle-reinforced mullite composite ceramic materials using kaolin and IG-017 bio-origin additives. Építőanyag – JSBCM Vol. 71 No. 4 p. 114 https://doi.org/10.14382/epitoanyag-jsbcm.2019.20

[11] Khare, S., Sharma, M., Venkateswarlu, K. (2010): Effect of scandium additions on pressure less sintering of Al-TiN metal matrix composites. Építőanyag, Vol. 61. No.2. pp. 39–42. http://dx.doi.org//10.14382/epitoanyag-jsbcm.2010.8

[12] Tamásné Csányi Judit, Gömze A. László (2008): Impact of nitrogen atmosphere on sintering of alumina ceramics. Építőanyag – JSBCM Vol. 60. No.1 p. 15 http://dx.doi.org/10.14382/epitoanyag-jsbcm.2008.4

[13] Kulkov, S. N., Dedova, E. S., Pedraza, F., Erdélyi, J. (2014): Porosity and Mechanical Properties of Zirconium Ceramics. Építőanyag – JSBCM, Vol. 66, No. 2 pp. 35–37. http://dx.doi.org/10.14382/epitoanyag-jsbcm.2014.7

[14] Zhengwei Nie, Yuyi Lin (2015): Fabrication of porous alumina ceramics with corn starch in an easy and low-cost way, Ceramics Silikaty Vol. 59 No.4 pp. 348-352

[15] K. Ornam, M. Kimsan, E. Cahyono (2015): Evaluation of alternative desing of hollow brick with sawdust as filler for home-made industry, Advances in Environmental and Agricultural Science, Vol. 32, pp.373-376 ISBN: 978-1-61804-270-5

[16] Zhibin Ma, Chaolu Wen, Kezhou Yan, Yanxia Guo, Fangqin Cheng (2019): Effects of reducing environment and fusible components on carbothermal reduction–nitridation reaction of coal gangue at high temperature under N_2 atmosphere, Ceramics International, Vol. 45, Issue 17, Part B, pp. 22829-22840, https://doi.org/10.1016/j.ceramint.2019.07.325

[17] M. N. Ismael, H. F. Hassan, H. S. Al-lami (2020): Effect of silica particle size on the physical and mechanical properties of lightweight ceramic composites, Revista de Chimie, Vol. 71. No. 5, pp. 65-74, https://doi.org/10.37358/RC.20.5.8114

[18] E. Kurovics, J. F. M. Ibrahim, M. Tihtih, B. Udvardi, K. Nuilek and L. A. Gömze (2020): Examination of mullite ceramic specimens made by conventional casting method from kaolin and sawdust, J. Phys.: Conf. Ser. Vol. 1527 012034 https://doi.org/10.1088/1742-6596/1527/1/012034

[19] L. A. Gömze, Á. Liszátzné Helvei, A. Simonné Odler, M. Szabó (2001): Ceramic yearbook I. 2001, ÉTK and MÉASZ, Budapest, ISBN 963 512 774 X pp.30-85

[20] Bobkova N. M. (2007): Fizicheskaya Himiya Tugoplavkih Nemetallicheskihi Silicatnyh Materialov, Yvyshej Shaya, Minszk, P. 88-90 ISBN 978-985-06-1389-9

[21] G Varga (2007): The structure of kaolinite and metakaolinite. Építőanyag, Vol. 59, No.1 p. 6 http://dx.doi.org/10.14382/epitoanyag-jsbcm.2007.2

[22] A Borosnyói, A. Szijártó (2016): Metakaolin vizsgálata cement kiegészítô anyagként a k-érték elve szerint. Építőanyag – JSBCM Vol. 68, No. 2 p. 40 http://dx.doi.org/10.14382/epitoanyag-jsbcm.2016.7

[23] G. Kakali, T. Perraki, S. Tsivilis, E. Badogiannis(2001): Thermal treatment of kaolin: the effect of mineralogy on the pozzolanic activity, Applied Clay Science, Vol. 20. No.1-2 pp. 73-80 https://doi.org/10.1016/S0169-1317(01)00040-0

[24] Wang, H., Li, C., Peng, Z. et al. (2011): Characterization and thermal behavior of kaolin. Journal of Thermal Analysis and Calorimetry Vol. 105. pp.157–160 https://doi.org/10.1007/s10973-011-1385-0

[25] F. Sahnoune, M. Chegaar, N. Saheb, P. Goeuriot, F. Valdivieso (2013): Differential thermal analysis of mullite formation from Algerian kaolin, Advances in Applied Ceramics, Structural, Functional and Bioceramics, Vol. 107 pp. 9-13 https://doi.org/10.1179/174367607X228007

[26] O. Castelein, B. Soulestin, J. P. Bonnet, P. Blanchar (2001): The influence of heating rate on the thermal behaviour and mullite formation from a kaolin raw material, Ceramics International, Vol. 27. No.5 pp. 517-522 https://doi.org/10.1016/S0272-8842(00)00110-3

[27] Petr Ptáček, Dana Kubátová, Jaromír Havlica, Jiří Brandštetr, František Šoukal, Tomáš Opravil (2010): Isothermal kinetic analysis of the thermal decomposition of kaolinite: The thermogravimetric study, Thermochimica Acta, Vol. 501. No.1-2 pp. 24-29 https://doi.org/10.1016/j.tca.2009.12.018

[28] Tomáš Ondro, Omar Al-Shantir, Štefan Csáki, František Lukáč, Anton Trník (2019): Kinetic analysis of sinter-crystallization of mullite and cristobalite from kaolinite, Thermochimica Acta Vol. 678. p. 178312 https://doi.org/10.1016/j.tca.2019.178312

[29] L A Gömze, S N Kulkov, E Kurovics, A S Buyakov, S P Buyakova, A Y Buzimov, R Géber, M V Grigoriev, I Kocserha, A S Kulkov, T Yu Sablina, N L Savchenko, I N Sevostyanova, A Simon (2018): Investigation of mineralogical composition and technological properties of conventional brick clays. Építőanyag – JSBCM Vol. 70. No.1 p. 8 https://doi.org/10.14382/epitoanyag-jsbcm.2018.2

[30] O Kotova (2013): Clay Minerals: Adsorbophysical Properties. IOP Conf. Ser.: Mater. Sci. Eng. Vol.47 012037 https://doi.org/10.1088/1757-899X/47/1/012037

[31] Š Csáki, I Štubňa, V Trnovcová, J Ondruška, L Vozár and P Dobroň (2017): Evolution of AC conductivity of wet illitic clay during drying. IOP Conf. Ser.: Mater. Sci. Eng.Vol. 175 012041 https://doi.org/10.1088/1757-899X/175/1/012041

[32] Alexandra Hamza and István Kocserha (2020): The effect of expanded perlite on fired clay bricks. J. Phys.: Conf. Ser. Vol. 1527, 012032 https://doi.org/10.1088/1742-6596/1527/1/012032

[33] Kurovics E., Gömze A. L. (2019): Thermo-analytical analysis of kaolin and bio-additive mixtures using a derivatograph and heating microscope. Preparation of Ceramic Materials Proceedings of Edited Contributions, p. 180 ISBN: 978-80-553-3314-4

Ref.:

Kurovics, Emese – **Kotova**, Olga B. – **Ibrahim**, Jamal Eldin F. M. – **Tihtih**, Mohammed – **Sun**, Shiyong – **Pala**, Péter – **Gömze**, László A.: *Characterization of phase transformation and thermal behavior of Sedlecky Kaolin*
Építőanyag – Journal of Silicate Based and Composite Materials, Vol. 72, No. 4 (2020), 144–147. p.
https://doi.org/10.14382/epitoanyag-jsbcm.2020.24

Szomorú szívvel tudatjuk mindazokkal, akik ismerték és szerették,
hogy életének 79. évében elhunyt

Dr. Arató Péter

fizikus, az MTA doktora.

Dr. Arató Péter Kaposváron született, 1941 szeptember 23-án.

1964-ben szerzett fizikus oklevelet, 1974-ben a fizikai tudományok kandidátusa lett, majd 1999-ben MTA doktori fokozatot szerzett, 2001-ben a Miskolci Egyetemen habilitált. 1982-ig a Csepeli Fémműben dolgozott, azóta a Műszaki Fizikai Intézetben (MÜFI) majd jogutódjában Műszaki Fizikai és Anyagtudományi Kutatóintézetben (MFA) dolgozott. Dr. Arató Péter vezette a Kerámia- és Fémfizikai Kutatások Osztályát, ahol a szilíciumnitrid kerámia és a kis méretű kerámiatestek előállításával foglalkozott. Az összetétel, az előállítási paraméterei, a kialakuló szerkezet és a mechanikai tulajdonságok kapcsolatrendszerének egyes problémáit tisztázva képes volt csapatával nagy szilárdságú és magas hőállóságú kerámiatestek gyártására, amelyeket a Tungsram-GE gyárai szerszámként alkalmaztak nagy mechanikus és termikus igénybevételnek kitett területeken.

A Szilikátipari Tudományos Egyesület Finomkerámia szakosztály örökös tagjaként kiemelkedő szakmai hozzáértéssel járult hozzá az egyesület szakosztályának iparági elismeréséhez. A kerámia kutatásban eltöltött 30 év alatt elsők között teremtette meg a hazai modern kerámiakutatás alapjait. Tagja volt az MTA Anyagtudományi és Technológiai Tudományos Bizottságának (MTA ATTB) és az Európai Kerámia Társaságnak (EcerS). „SZILIKÁTIPARÉRT” Emlékérem birtokosa. Szakmai tevékenysége eredményeként a kutatás és fejlesztések eredményei a finomkerámia iparban is hasznosultak. Több szakmai kéziratot és szabadalmat publikált és több hazai és nemzetközi fórumon tartott szakmai előadást, a finomkerámiai anyagok és technológiák elterjesztése érdekében. 1986–2012 között 55 szakcikkben, 14 könyvrészletben és 19 egyéb konferencia közleményben foglalkozott kutatási eredményeivel, ezekben egyaránt útmutatást adott a finomkerámia ipar és a fiatal kutatók számára.

2020 április 28-án búcsúzott el szeretett családjától.

Nyugodjék békében!
Emlékét szeretettel őrizzük szívünkben.

SZTE

Megrendülten fogadtuk, hogy

Dr. Révay Miklós

a magyar cement-, beton- és mészipar meghatározó személyisége 2020. május 11-én elhunyt.

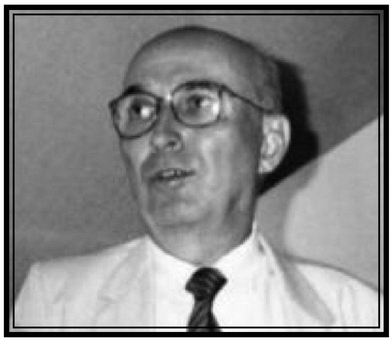

Dr. Révay Miklós egy olyan korban született, amely generációnak a legnehezebb körülmények között kellett elindítania, majd felépítenie életét, viharos történelmi időszakok váltakozása közepette. Ő mindezek ellenére odáig jutott, hogy szorgalmával és a szakmába vetett hitével az iparág egyik meghatározó alakjává vált.

1958-ban a Veszprémi Egyetem Szilikát Tanszék kötőanyag tagozatán szerzett vegyészmérnöki diplomát, majd 1964-ben műszaki doktor címet. 1974-ben a Mengyelejevről elnevezett Kémiai Technológiai Egyetemen szerezett kémiatudomány kandidátusa fokozatot. Érdeklődése a kötőanyagok iránt, a műszaki fejlődés határainak feszegetése, a kutatói tevékenység iránti elhivatottsága már egyetemista korában felébredt benne. Tanára, Bereczky Endre már korán felismerte a kutatói munkára való rátermettségét, meghatározta dr. Révay Miklós szakmai sorsát, ugyanis 1962-ben „zseniális fickó"-ként ajánlotta Beke Bélának a SZIKKTI (akkoriban ÉaKKI) cementkutató osztályára. Kutatói pályafutása 1991-től a Cementipari Kutató és Fejlesztő Kft.-ben folytatódott 1995-ös nyugdíjba vonulásáig. Nyugdíjasként sem pihent, amíg egészsége engedte tovább dolgozott a CEMKUT Kft-ben tudományos tanácsadóként. Tudása egészen kivételes volt, folyamatosan tanult és dolgozott, nem sajnálta az időt arra, hogy minél jobban kiismerje szakmája minden területét, és irányt mutasson az új felfedezésére.

Színes szakmai életútja, munkássága során számos cementkémiai és -technológiai kérdéssel foglalkozott. A tudományos eredmények között ki kell emelni – az aluminátcement hidratációja, ill. szilárdulása során végbemenő fizikai-kémiai folyamatok elméleti tanulmányozására irányult kutatásokat, amelyek alapján olyan vizsgálati módszert fejlesztett ki, melynek segítségével a bauxitbetonok, ill. a belőlük készült műtárgyak időállósága, élettartama prognosztizálható. Ezen tudományos eredményei nemzetközileg is elismerést nyertek. Hazánkban és külföldön is számos bauxitbetonból készült épület életben maradását a „Révay-prognózisnak" köszönheti. Maradandót alkotott a cementek szulfátállóságának, gőzölhetőségének, a tűzállócementek és betonok alkalmazástechnikai tulajdonságainak kutatása terén is. Foglalkozott az útépítési cementekkel, és az ő kutatásai alapozták meg a már-már elfelejtett trasszportlandcementek gyártásának újbóli hazai bevezetését. Szinte egyedüli művelője volt a mészipari kutatásoknak hazánkban. Kiemelkedő szerepe volt a cement-, beton- és mészipari szabványok kidolgozásában, nemzetközi szabványok honosításában is. Kutatási eredményeit hazai és külföldi folyóiratokban több, mint száz publikációban tette közzé. Rendszeres előadója volt olyan hazai és nemzetközi tudományos rendezvényeknek, mint a cement, mész, beton, tűzállóanyag, vagy termoanalitikai konferenciák és kongresszusok.

Mindig jelentős szerepet vállalt a közösségi, ill. társadalmi életben. A SZIKKTI Tudományos Tanács titkára, az MTA számos Bizottságának, az „Építőanyag" és „Beton" szaklapok szerkesztőbizottságának tagja, rendszeresen publikáló szerzője volt.

Nyugodjék békében!
Emlékét szeretettel őrizzük szívünkben.

SZTE

GUIDELINE FOR AUTHORS

The manuscript must contain the followings: title; author's name, workplace, e-mail address; abstract, keywords; main text; acknowledgement (optional)**; references; figures, photos with notes; tables with notes; short biography** (information on the scientific works of the authors).

The full manuscript should not be more than 6 pages including figures, photos and tables. Settings of the word document are: 3 cm margin up and down, 2,5 cm margin left and right. Paper size: A4. Letter size 10 pt, type: Times New Roman. Lines: simple, justified.

TITLE, AUTHOR

The title of the article should be short and objective.

Under the title the name of the author(s), workplace, e-mail address.

If the text originally was a presentation or poster at a conference, it should be marked.

ABSTRACT, KEYWORDS

The abstract is a short summary of the manuscript, about a half page size. The author should give keywords to the text, which are the most important elements of the article.

MAIN TEXT

Contains: materials and experimental procedure (or something similar), results and discussion (or something similar), conclusions.

REFERENCES

References are marked with numbers, e.g. [6], and a bibliography is made by the reference's order. References should be provided together with the DOI if available.

Examples:

Journals:

[6] Mohamed, K. R. – El-Rashidy, Z. M. – Salama, A. A.: In vitro properties of nano-hydroxyapatite/chitosan biocomposites. *Ceramics International*. 37(8), December 2011, pp. 3265–3271, http://doi.org/10.1016/j.ceramint.2011.05.121

Books:

[6] Mehta, P. K. – Monteiro, P. J. M.: Concrete. Microstructure, properties, and materials. *McGraw-Hill*, 2006, 659 p.

FIGURES, TABLES

All drawings, diagrams and photos are figures. The **text should contain references to all figures and tables**. This shows the place of the figure in the text. Please send all the figures in attached files, and not as a part of the text. **All figures and tables should have a title**.

Authors are asked to submit color figures by submission. Black and white figures are suggested to be avoided, however, acceptable.

The figures should be: tiff, jpg or eps files, 300 dpi at least, photos are 600 dpi at least.

BIOGRAPHY

Max. 500 character size professional biography of the author(s).

CHECKING

The editing board checks the articles and informs the authors about suggested modifications. Since the author is responsible for the content of the article, the author is not liable to accept them.

CONTACT

Please send the manuscript in electronic format to the following e-mail address: femgomze@uni-miskolc.hu and epitoanyag@szte.org.hu or by post: Scientific Society of the Silicate Industry, Budapest, Bécsi út 122–124., H-1034, HUNGARY

We kindly ask the authors to give their e-mail address and phone number on behalf of the quick conciliation.

Építőanyag – *Journal of Silicate Based and Composite Materials*, Quarterly peer-reviewed periodical of the Hungarian Scientific Society of the Silicate Industry, SZTE. http://epitoanyag.org.hu